Delft University of Technology
Master of Science Thesis in Computer and Embedded Systems Engineering

Prediction based approach to handover mechanism for hybrid optical wireless networks utilizing narrow beams

Cleo Barik

Embedded Systems

TU Delft Delft University of Technology

Prediction based approach to handover mechanism for hybrid optical wireless networks utilizing narrow beams

Master of Science Thesis in Computer and Embedded Systems Engineering

Embedded Systems Group
Faculty of Electrical Engineering, Mathematics and Computer Science
Delft University of Technology
Van Mourik Broekmanweg 6, 2628 XE Delft, The Netherlands

Cleo Barik
m.s.barik@student.tudelft.nl
malab@outlook.com

August 20, 2025

Author
Cleo Barik (m.s.barik@student.tudelft.nl)
(malab@outlook.com)
Title
Prediction based approach to handover mechanism for hybrid optical wireless networks utilizing narrow beams
MSc Presentation Date
August 26, 2025

Graduation Committee

Qing Wang	Delft University of Technology
Remco Litjens	Delft University of Technology
Haibin Zhang	TNO

Abstract

This thesis presents mobility-aware handover mechanisms for hybrid radio frequency (RF) and narrow-beam optical wireless communication (NB-OWC) networks in indoor environments. Reactive handover mechanisms, commonly used in existing system such as Wi-Fi or hybrid Li-Fi and Wi-Fi networks HLWNets, are shown to be inadequate in ultra-dense NB-OWC deployments due to the limited coverage area per beam. To address these limitations, three novel handover mechanisms—one reactive and two predictive—were developed and evaluated against a baseline reactive mechanism from the literature.

A simulation framework assessed performance across a range of user speeds, using average throughput, lower-bound throughput, and handover rate as key metrics. The predictive mechanisms demonstrated significant improvements over reactive approaches, with the predictive throughput mechanism achieving a 157% increase in average throughput compared to the baseline. A trade-off between average and lower-bound throughput was observed, and a strong correlation between handover rate and throughput was identified.

These results demonstrate that prediction-based handover strategies can substantially enhance user experience and network efficiency in hybrid RF/NB-OWC systems, particularly under moderate mobility, and provide a foundation for exploring multi-user and more realistic deployment scenarios.

Preface

I am pleased to present this thesis, titled "Prediction-Based Approach to Handover Mechanism for Hybrid Optical Wireless Networks Utilising Narrow Beams," as the culmination of my Master's degree at Delft University of Technology, specialising in Computer Engineering and Embedded Systems.

Before pursuing this master's programme, I completed my bachelor's degree in Computer Communication Engineering. During my bachelor's thesis at Astrome Incorporated, I was first exposed to the cutting-edge developments in mobile networks, working on one of the first 5G mm-wave backhaul devices. This experience sparked my fascination with mobile network advancements, and since then, I have been eager to contribute to future network research.

I am genuinely grateful to The Netherlands Organisation for Applied Scientific Research (TNO) for providing me with the opportunity to undertake this thesis internship and for fostering a research environment that made this work possible. I extend my deepest gratitude to my company supervisors at TNO, Dr Haibin Zhang and Lotte Paulissen, for their invaluable guidance, patience, and support throughout this project. I also thank Robbert Schulpen, whose assistance was instrumental alongside Haibin and Lotte. My sincere appreciation goes to my university supervisor, Dr Qing Wang, for his insightful feedback and encouragement.

I am thankful to my fellow interns and friends for their camaraderie and support, which made this journey more rewarding and comforting far from home.

Most importantly, I am profoundly grateful to my family for their unwavering moral and financial support throughout these two years. Their belief in me has been my greatest strength.

This thesis is a collective achievement, reflecting the dedication, encouragement, and support of many people. I wholeheartedly dedicate it to all who have contributed to this journey, whether through guidance, friendship, or unwavering belief in my abilities.

Finally, I acknowledge the use of Microsoft Copilot to refine the language of this thesis, limited to spelling, grammar, and tone adjustments.

Cleo Barik

Delft, The Netherlands
20th August 2025

Acronyms

2D 2-dimensional.

6G sixth generation.

A-TCNN attention-based temporal convolutional neural network.

AADR average available data rate.

ADR angle diversity receiver.

AP access point.

AWGN additive white gaussian noise.

AWGR arrayed waveguide grating router.

BER bit error rate.

CCR corner cube retroreflector.

CPC compound parabolic concentrators.

DC direct current.

DCO DC-biased optical.

DMT discrete multitone.

FEC forward error correction.

FSOC free space optical communication.

GOB grid-of-beams.

HetNets heterogeneous networks.

HHO horizontal handover.

HLWNets hybrid Li-Fi and Wi-Fi networks.

IM-DD intensity modulation, direct detection.

IoT internet of things.

IR infrared.

IS image sensor.

LD laser diode.

LED light emitting diode.

LoS line-of-sight.

MIMO multiple-input multiple-output.

NB-OWC narrow-beam optical wireless communication.

NLoS non-line-of-sight.

OCC optical camera communication.

OFDM orthogonal frequency division multiplexing.

OOK on-off keying.

OWC optical wireless communication.

PAM pulse amplitude modulation.

PD photodiode.

PSD power spectral density.

QoS quality of service.

R&D research and development.

RF radio frequency.

RIN relative intensity noise.

RSS received signal strength.

RWP random waypoint.

SINR signal-to-interference-plus-noise ratio.

SMF single mode fiber.

SNR signal-to-noise ratio.

TIA transimpedance amplifier.

UD user device.

UE user equipment.

UV ultraviolet.

VCSEL vertical-cavity surface-emitting Laser.

VHO vertical handover.

VL visual light.

VLC visual light communication.

VR virtual reality.

VR/XR virtual and extended reality.

WBAN wireless body area network.

WLAN wireless local area network.

WPAN wireless personal area network.

Contents

List of Figures

List of Tables

Chapter 1

Introduction

1.1 Motivation

The rapid growth in mobile data traffic, along with the widespread adoption of mobile devices and cellular subscriptions, has placed considerable strain on traditional radio frequency (RF) networks [3]. As users increasingly demand high-speed connectivity in both outdoor and indoor environments, the pressure extends beyond cellular networks alone. This surge in demand has driven the dense deployment of Wi-Fi hotspots, which are projected to reach 950 million globally in 2025 and to 3.15 billion globally by 2030 [53]. However, the limited availability of RF spectrum has led to intense competition for channels, making it increasingly difficult for RF systems to support the escalating data traffic. Future sixth generation (6G) wireless communication systems aim to address these limitations by offering among others higher data rates, lower end-to-end latency, and enhanced support for high-mobility users [4]. Meeting these goals within the constraints of the existing RF spectrum becomes increasingly infeasible, and requires the integration of complementary technologies.

Optical wireless communication (OWC) presents a promising alternative to traditional RF systems, particularly in indoor environments or short communication distance. OWC systems utilize the vast, unlicensed optical spectrum, which includes visible and infrared light, to provide significantly higher bandwidth than the congested RF spectrum [51]. Furthermore, OWC systems offer enhanced physical layer security, as optical signals cannot penetrate walls and other opaque barriers. This spatial confinement reduces the risk of external eavesdropping and enhances communication privacy. Moreover, the directional nature of optical beams improves energy efficiency by focusing power exclusively in the intended direction, thereby minimizing energy waste [48].

OWC becomes particularly effective when deployed as ultra-dense networks utilizing narrow optical beams. A notable advancement in this area is the use of laser-based optical sources, which enable highly focused, high-power transmissions capable of supporting network capacities in the terabit per second range [50]. Such narrow-beam laser systems offer exceptional spectral efficiency, making them well-suited for data-intensive applications. This architecture also improves spectral reuse and minimizes inter-cell interference, which is critical for high data rate, low-latency use cases such as virtual reality (VR). Addition-

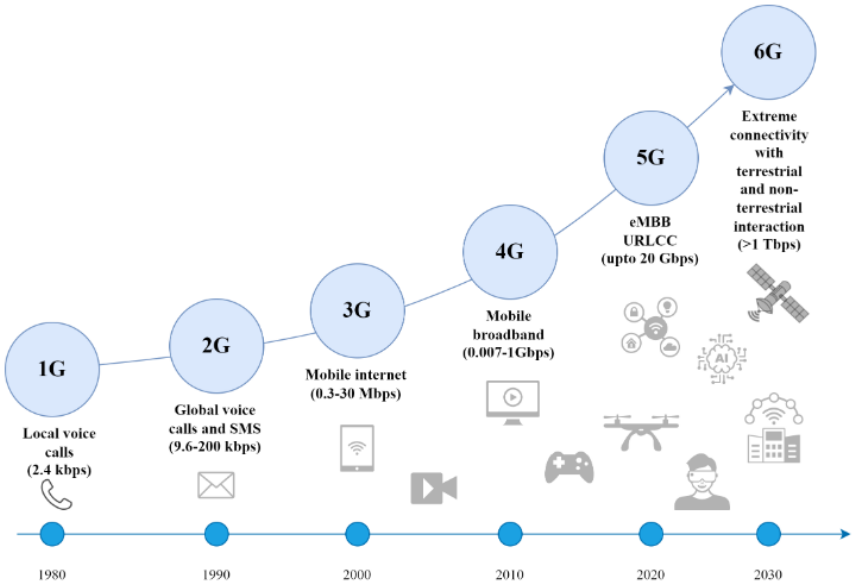

Figure 1.1: **Evolution of mobile networks: 1G to 6G [9]**

ally, the confined nature of narrow-beam transmissions enhances physical layer security by reducing the risk of interception or interference [13].

While NB-OWC systems offer remarkable advantages in terms of capacity, efficiency, and security, their practical deployment still faces several challenges that must be addressed. A primary limitation is their reliance on line-of-sight (LoS) conditions, as optical signals are easily blocked by physical obstacles. This sensitivity to obstructions reduces the reliability of OWC in dynamic environments with frequent user mobility [75]. Furthermore, the coverage range of NB-OWC is typically limited to just a few meters per AP, which constrains its effectiveness in larger indoor spaces [47]. In ultra-dense deployments, users often transition between small cells, resulting in frequent handovers. These handovers increase the likelihood of service interruptions and can degrade overall quality of service (QoS) performance [75]. Therefore, efficient handover management is critical to ensuring seamless connectivity and maintaining high network performance.

Integrating RF and OWC technologies into hybrid communication systems enables the complementary strengths of both to be harnessed. RF technologies, such as Wi-Fi, offer broader coverage and the ability to penetrate obstacles, making them ideal as a fallback in non-line-of-sight (NLoS) scenarios. Hybrid systems that combine RF and OWC can deliver the high data rates and low latency of optical communication while ensuring robust and continuous coverage through RF.

However, managing hybrid systems introduces significant complexity. Seamless switching between RF and OWC requires effective coordination and control mechanisms. To address this, it is essential to continue research focused on developing intelligent algorithms and adaptive policies that can dynamic-

ally manage connectivity based on user mobility, environmental conditions, and application requirements. Such solutions are essential to achieving optimal performance and uninterrupted service in heterogeneous networks.

Among the most pressing challenges in hybrid optical-RF networks is effective mobility management, particularly regarding the handover processes. Seamless transitions between APs or communication technologies (such as from OWC to RF or vice versa) are inherently complex due to the distinct physical characteristics of each medium.

To ensure consistently high QoS performance and user experience in such heterogeneous environments, robust handover mechanisms are crucial. These mechanisms should account for a range of dynamic factors, including user mobility patterns, link stability, and the specific requirements of different applications. Addressing these variables is essential for enabling uninterrupted connectivity and optimal performance in next-generation wireless networks.

1.2 Research questions

A key distinguishing feature of NB-OWC systems, compared to traditional wireless networks, is the extremely limited coverage area of each individual optical beam. While conventional RF networks (e.g., Wi-Fi) may have a diameter in the scale of tens of metres per cell, NB-OWC systems often operate with beam diameters as small as ten centimetres. This significant reduction in per-beam coverage presents a unique challenge. Existing handover mechanisms, which typically rely on reactive mechanisms based on periodic signal measurements, are not well-suited to environments where users may cross multiple beams in rapid succession. Even modest user movement can trigger frequent handovers, leading to increased signalling overhead and potential service disruptions.

This observation motivates the central research questions addressed in this thesis:

- *How can handover mechanisms be redesigned to accommodate the ultra-dense deployment and limited per-beam coverage of NB-OWC networks?*
- *What predictive or proactive mechanisms can be employed to ensure seamless connectivity and maintain quality of service performance?*
- *How does the proposed approach compare to existing solutions in the literature in terms of user experience performance?*

1.3 Key contributions

This thesis makes the following key contributions to the field of handover management in hybrid RF-NB-OWC systems:

- **Design of predictive handover mechanisms:** The primary contribution of this work is the design of a novel set of predictive handover mechanisms specifically developed for hybrid RF/OWC systems employing narrow-beam optical links. To the best of the author's knowledge, this is the first study to introduce predictive handover mechanisms that directly address the challenges associated with the extremely limited coverage area of individual beams of NB-OWC systems.

- **Performance evaluation against baseline approach:** The proposed handover mechanisms are evaluated against a baseline reactive approach adapted from existing hybrid RF-Optical systems [76]. Simulation results demonstrate that the predictive mechanisms outperform the baseline in terms of the overall user experienced throughput.
- **Development of a custom simulation framework:** A customized simulation environment was designed and implemented to model hybrid RF/NB-OWC networks and evaluate handover performance under realistic mobility conditions. This framework supports flexible experiments and can serve as a foundation for future research in this area.

1.4 Structure of the thesis

The rest of the thesis is organized as follows:

- **Chapter 2: Background -** provides the necessary background and reviews related work in the field. It highlights the limitations of existing approaches and identifies the research gap that this thesis addresses.
- **Chapter 3: System modelling -** presents the system modelling for both RF and OWC networks. It also defines the evaluation parameters used in the study, including signal-to-noise ratio (SNR), signal-to-interference-plus-noise ratio (SINR), and estimated throughput.
- **Chapter 4: Handover mechanism design -** details the implementation of the handover mechanisms developed and evaluated in this work.
- **Chapter 5: Evaluation setup and results -** describes the simulation setup, including the scenario configuration and the baseline method used for comparison. It also presents and analyses the results obtained from the simulations.
- **Chapter 6: Conclusions -** discusses the conclusions drawn from the results presented in Chapter 5. It further outlines potential directions for future research in this area based on the conclusions and limitations of the thesis.
- **Appendix A:** addresses discrepancies observed between the implemented optical model and the reference model from the literature. It provides explanations for these differences and includes validation tests to support the correctness of the implementation.

Chapter 2

Background

This chapter presents the foundational background necessary to contextualize the proposed work. It begins with an overview of OWC, establishing its relevance and distinguishing characteristics. The discussion then narrows in scope to address narrow-beam optical links and the integration of OWC and RF systems in hybrid network architectures. Relevant prior research is reviewed, with a focus on identifying limitations and open challenges. These observations collectively underscore the motivation for this thesis and highlight the specific contribution it makes within the field.

2.1 Optical wireless communication

OWC has been an area of research since at least the 1960s, with early efforts including NASA's investigations into ground-to-satellite optical links in the 1970s, culminating in the first successful demonstration in 1995 [69]. In parallel, researchers at IBM explored the viability of infrared transmission for computer networking applications [58]. The early 2000s saw accelerated progress in the development of practical OWC systems, bolstered in part by advancements in the terrestrial optical fibre industry. Over the past two decades, OWC research and development (R&D) has expanded rapidly, driven by two converging trends: the exponential growth in mobile data demand [2] and the decreasing cost and increasing availability of commercial off-the-shelf optical components [51].

Today, OWC is an increasingly mature technology, with industrial applications including high-throughput inter-satellite links such as those used by Starlink [18]. Research and development in the field continues at a steady pace, driven in part by the growing momentum toward next-generation wireless standards, including 6G and beyond. These emerging standards place heightened demands on network infrastructure, emphasizing ultra-high data rates, ultra-low latency, and ubiquitous connectivity. OWC is well-positioned to address these challenges due to several inherent advantages: access to a vast unlicensed optical spectrum, strong physical layer security, and a robust, rapidly evolving ecosystem of optical components. Furthermore, OWC exhibits remarkable scalability, supporting use cases that range from on-chip optical interconnects to long-range deep space communication. As such, OWC stands as a compelling candidate for supplementing and, in certain contexts, redefining the future landscape of

wireless communication systems.

2.1.1 Categories of OWC technologies

OWC encompasses a broad set of technologies that use light for wireless data transmission. To contextualize their capabilities, this section classifies OWC systems by communication distance, spectral band, and enabling technologies. These categories reveal the diversity of OWC applications—from chip-level links to satellite communications—and highlight the trade-offs across visible, infrared, and ultraviolet bands. This section also outlines key differences among visual light communication (VLC), Li-Fi, optical camera communication (OCC), and free space optical communication (FSOC), leading into a focused discussion on medium-range, infrared (IR)-based Li-Fi systems for short-distance environments.

Categorization based on communication distance

Based on transmission distance, OWC systems are typically classified into five categories: ultra-short range, short range, medium range, long range, and ultra-long range [21].

- **Ultra-short range systems** operate at nanometre to millimetre scales and are primarily used for inter-chip communication, where high-speed data transfer is required between integrated circuit components [6].
- **Short-range systems** typically function over centimetre-level distances and are suited for applications such as wireless body area network (WBAN) and wireless personal area network (WPAN), where compact, low-power communication links are essential [19].
- **Medium-range systems** span distances on the order of meters and are comparable in scope to traditional wireless local area network (WLAN) [26]. This category includes a substantial portion of both commercial and academic efforts in VLC and Li-Fi, due to their suitability for indoor environments and high-capacity user access [79].
- **Long-range systems** operate at distances ranging from hundreds of meters to several kilometres and are envisioned for use in inter-building communication and wireless optical backhaul, particularly where laying fibre is impractical or cost-prohibitive [44].
- **Ultra-long range systems** enable point-to-point links between satellites or between satellites and ground stations, representing a key enabler for high-throughput FSOC in space-based networks [16].

Categorization based on spectrum utilized

From the perspective of spectral utilization, OWC systems are generally categorized into three main bands: IR, visual light (VL), and ultraviolet (UV):

- **Visible light** systems are extensively employed in ongoing development in VLC, Li-Fi, and OCC, particularly in indoor environments where light

sources serve the dual purpose of illumination and data transmission [30]. This dual functionality offers certain advantages, such as seamless integration into existing lighting infrastructure, thereby lowering the barrier to adoption. However, this also introduces limitations. Since the system relies on illumination, data transmission is constrained by lighting requirements. Data links must remain active even during periods when illumination is unnecessary [24]. In case of intensity modulation, direct detection (IM-DD) systems, extra attention needs to provided to avoid the phenomenon of visual flickering during data transmission. data integrity techniques like dithering need to be used to encode data within imperceptible variations in light intensity [14].

- **IR systems** are among the earliest OWC technologies to be experimentally validated. As early as in the 1980s, IR links were employed to demonstrate successful data transmission, albeit at relatively low data rates. Today, IR-based communication systems span a broad range of applications, from short-range links to long-range terrestrial point-to-point systems [68]. The IR spectrum is particularly favoured in outdoor and high-capacity backhaul scenarios due to its ability to support high data rates while remaining immune to interference from visible light sources [10].

  Recent developments in Li-Fi architectures have seen a shift from single wide-beam illumination toward multibeam, narrow-angle transmission using IR lasers. This architectural shift has enabled per-user data rates in the order of multiple gigabits per second, with aggregate network capacities exceeding a terabit per second, depending on beamforming and spatial multiplexing techniques [47] [41].

  A key advantage of IR lies in its invisibility to the human eye, which eliminates issues such as visual flickering that are inherent to visible light communication systems. However, this also necessitates careful adherence to eye safety standards. Exceeding regulated power density thresholds in IR transmissions can pose a risk of retinal damage, especially when laser-based sources are used, prompting the need for eye-safe design considerations and compliance with standards such as IEC 60825-1 [7]

- **UV systems** are of particular interest in scenarios where NLoS communication is essential. Unlike visible and IR systems, which primarily rely on direct line-of-sight transmission, UV systems can exploit atmospheric scattering to establish communication links even in obstructed environments [81]. This is typically achieved through the use of intersecting beams from the transmitter and receiver, relying on the scattered photons within the UV band to carry the signal across indirect paths [29].

  Achieving high data rates in such systems, however, requires prior knowledge of the relative positions and alignment of both transmitter and receiver beams, which constrains the range of practical applications. As such, while UV OWC has been primarily investigated within the context of FSOC, particularly for outdoor and tactical networks [17]. Emerging research has begun exploring its integration into Li-Fi architectures, especially for enhancing coverage in NLoS indoor environments [85].

  A critical consideration in UV-based communication is safety. UV radiation, especially in the UV-C and UV-B ranges, can pose significant

Table 2.1: **Basic components for downlink communication in different OWC technologies.**

Technology	**Channel**	**Physical Tx**	**Physical Rx**
VLC	VL	LED	PD/Camera
Li-Fi	IR/VL	LED/LD	PD
OCC	IR/VL	LED	IS/Camera
FSOC	IR/VL/UV	LD	PD

biological risks, including skin and eye damage. Therefore, the use of protective equipment for personnel, along with robust shielding strategies, is essential. These are typically guided by regulatory recommendations from institutions such as the National Institute for Occupational Safety and Health (NIOSH) and international standards for occupational exposure limits [5].

Categorization based on enabling technology

OWC systems can also be classified based on their underlying enabling technologies, with the most commonly recognized categories being VLC, Li-Fi, OCC, and FSOC. While these technologies may utilize similar transmitter and receiver components (such as light emitting diode (LED)s, laser diode (LD)s, photodiode (PD)s, or image sensors), they differ in architecture, application domain, and operational principles. Despite often operating within overlapping spectral bands and transmission ranges, each technology serves distinct communication scenarios. Table 2.1 outlines the core similarities and differences among these technologies, focusing on the spectral band used, and the types of transmitter and receiver elements employed.

- **VLC** has emerged as a promising technology over the past decade. VLC systems operate exclusively within the visible light spectrum, typically utilizing LEDs for both illumination and data transmission. A defining characteristic of VLC is its emphasis on the dual-purpose use of lighting infrastructure, enabling simultaneous support for lighting and high-speed wireless communication [46]. This inherent synergy with pre-existing illumination systems makes VLC especially well-suited for high-density, short-range indoor environments, such as homes, offices, and enclosed vehicles including cars, aeroplanes, and trains [59].

  The reuse of lighting infrastructure offers tangible cost and energy efficiencies, further enhancing the appeal of VLC. Moreover, VLC is particularly advantageous in RF-restricted environments, such as hospitals and medical facilities, where electromagnetic compatibility is critical [72]. Since VLC operates solely within the visible light spectrum, it is generally considered safe for human exposure, unlike some infrared or ultraviolet-based technologies. This safety is largely attributed to the very low power density levels typically used in VLC systems, which contrast with certain infrared systems that can emit potentially hazardous power densities.

  Despite these strengths, VLC also presents several limitations. Its short operational range, typically less than 10 meters, restricts its use to confined

spaces [20]. Additionally, VLC is unsuitable for most outdoor scenarios, due to high susceptibility to interference from ambient sunlight. Furthermore, as a LoS communication system, VLC is sensitive to obstructions and less reliable in dynamic environments where users or objects may frequently block the optical path [59].

- **Li-Fi** is often used interchangeably with VLC; however, there are key distinctions that set it apart as a more comprehensive wireless networking solution. While VLC systems are typically unidirectional and primarily confined to the visible light spectrum, Li-Fi systems are inherently bidirectional and are not restricted to visible wavelengths [23]. Recent advancements have increasingly incorporated IR light, expanding the operational flexibility of Li-Fi beyond traditional VLC constraints [66]. Like VLC, Li-Fi systems commonly use LEDs as transmitters, benefiting from their energy efficiency and fast switching capabilities.

  Unlike VLC, which can function in simple point-to-point configurations and does not inherently support mobility [22], Li-Fi is designed to operate in point-to-multipoint and multipoint-to-point topologies. This enables seamless user mobility and dynamic handover, positioning Li-Fi as a full-fledged wireless networking system comparable in scope to Wi-Fi [31]. Furthermore, Li-Fi systems are increasingly leveraging LD, particularly VCSEL and tunable lasers, to achieve significantly higher data rates. Demonstrations have shown throughput exceeding 56 Gb/s, highlighting Li-Fi's potential for high-capacity, low-latency communication [54].

  Li-Fi also introduces a new paradigm in heterogeneous multi-tier network architectures through the concept of attocells. These are ultra-small optical cells that generate no RF interference and coexist harmoniously with existing femtocells and Wi-Fi networks [79]. Despite these advantages, Li-Fi shares several limitations with VLC, such as its reliance on LoS communication, which makes it vulnerable to obstructions. Additionally, when operating in the visible spectrum, it remains unsuitable for outdoor environments due to ambient light interference [30]. Its effective range is also typically limited to short-range indoor scenarios.

- **OCC** is a distinctive subclass of OWC that utilizes light sources such as LEDs as transmitters and image sensor (IS) or cameras as receivers [27].OCC systems leverage the widespread presence of cameras in consumer devices, allowing for low-cost and hardware-free deployment in smartphones, tablets, and other smart electronics [15]. OCC can operate in both the VL and IR bands, although it is generally limited to using LEDs as transmitters.

  A key advantage of OCC is its ability to achieve robust communication in high-noise environments, such as those with ambient sunlight or artificial lighting [61]. The use of image sensors enables non-interfering multi-source communication by spatially separating light signals on the camera's focal plane, which significantly improves signal quality and SNR [36]. Moreover, OCC systems are inherently resistant to variations in communication distance, provided the LED remains resolvable within the sensor's pixel grid. These features eliminate the need for complex filtering or signal processing,

making OCC an attractive solution for low-complexity, spatially multiplexed applications.

However, OCC also faces notable limitations. It is currently constrained by low data rates, primarily due to the limited frame rates of commercial cameras, which hinders support for high-throughput communication. Additionally, OCC systems are susceptible to visible flickering, especially at low transmission frequencies, and require LoS paths between transmitter and receiver [82]. These drawbacks restrict OCC's applicability in scenarios demanding high-speed, long-range, or flicker-free operation.

- **FSOC** is a high-capacity OWC technology that primarily operates in the IR spectrum, though it can also utilize VL and UV bands depending on the application [44]. What sets FSOC apart from other OWC technologies is its reliance on highly focused, narrow laser beams—typically from LD to establish long-range, LoS communication links between fixed points [45]. FSOC systems can achieve data rates comparable to fibre optics, with demonstrated throughputs exceeding 10 Gb/s and potential applications over distances ranging from a few meters to several kilometres [71].

  The absence of spectrum licensing and the ability to rapidly deploy FSOC links make the technology particularly attractive for cellular backhaul, disaster recovery, secure point-to-point links, and inter-building connectivity. FSOC is also widely applicable in specialized domains such as satellite-to-ground, aircraft-to-aircraft, and ship-to-ship communication, where traditional wired, or RF solutions may be infeasible [39].

  Despite these strengths, FSOC faces significant limitations, particularly in terms of link reliability. The performance of FSOC links is highly susceptible to atmospheric disturbances such as fog, rain, haze, and turbulence, which can attenuate or distort the optical signal [12]. Physical obstructions, including buildings or moving objects like birds, can momentarily disrupt communication due to the system's strict reliance on a clear LoS. As a result, although FSOC offers high-speed and long-range potential, it requires careful alignment, environmental monitoring, and potentially backup systems to ensure robust performance in dynamic or harsh conditions.

While each enabling technology within the OWC domain offers unique advantages and application scenarios, this thesis specifically focuses on medium-range Li-Fi systems in indoor environments utilizing the IR spectrum. The choice is motivated by Li-Fi's bidirectional communication capabilities, support for user mobility, and its potential to serve as a high-capacity, low-latency wireless networking solution.

2.2 Narrow-beam optical wireless communication

Building upon the focus on Li-Fi systems in indoor environments, recent advancements have increasingly explored the use of NB-OWC, particularly within the IR spectrum. These systems have demonstrated significant potential for

delivering ultra-high-speed wireless connectivity in medium-range indoor scenarios. By directing highly focused IR laser beams toward mobile devices, IR systems are capable of achieving multi-gigabit per second data rates per user, offering a compelling alternative to conventional RF-based technologies.

The use of narrow beams introduces several key advantages, including spatial diversity, reduced interference, and enhanced physical layer security. These attributes make NB-OWC particularly attractive for high data-rate demanding applications such as virtual and extended reality (VR/XR), as well as dense multi-user environments like meeting rooms and collaborative workspaces. As the demand for immersive and high data-rate services grows, NB-OWC stands out as a promising candidate for next-generation indoor wireless networks.

A fundamental challenge in NB-OWC systems arises from the limited coverage area of each beam, which necessitates precise alignment between the and the user device to establish and maintain a reliable communication link. This requirement becomes particularly critical in dynamic indoor environments where user mobility is a key consideration.

To address this challenge, the literature identifies two primary architectural approaches for managing beam alignment and user connectivity. These approaches form the basis for a broad classification of NB-OWC systems into:

- **Beam Steering Systems**, which dynamically direct a single or limited number of beams toward users in real time.
- **Static Grid-of-Beams Systems**, which deploy a dense, fixed array of narrow beams to cover the entire service area without requiring active steering.

Each of these paradigms offers distinct trade-offs in terms of complexity, scalability, responsiveness to mobility, and system cost. The following subsections explore these two classifications in greater detail.

2.2.1 Beam steering system

Beam steering systems have been central to the development of NB-OWC, particularly in efforts to support user mobility and dynamic link establishment. These systems employ mechanisms to dynamically direct narrow optical beams—typically in the IR spectrum—toward mobile user devices, ensuring that the LoS link is maintained as users move within the coverage area [48].

A notable example of this approach is the use of wavelength-tunable diffractive optics, as demonstrated by Koonen et al. [50] In their work, a passive diffractive optical module composed of crossed grating elements enables two-dimensional 2-dimensional (2D) beam steering by varying the wavelength of the laser source. This technique allows for precise control of IR pencil beams—highly collimated beams with minimal divergence—without the need for mechanical movement. Using this method, the authors achieved downstream data rates of 32 Gb/s and 42.8 Gb/s per beam over a three-metre range, employing 4-pulse amplitude modulation (PAM) and adaptive discrete multitone (DMT) modulation, respectively, at a wavelength of 1550 nm.

An alternative wavelength-controlled steering method involves the use of arrayed waveguide grating router (AWGR)s. In another study by Koonen et al. [49], a high port-count AWGR was used to steer IR pencil beams by routing

distinct wavelengths through a bundle of single mode fiber (SMF)s. The output fibres were arranged in a 2D square array and paired with a lens, enabling beam direction control by adjusting the array's position relative to the lens. This configuration demonstrated 112 Gb/s 4-PAM transmission over a 2.5-metre reach using an 80-port C-band AWGR, with an estimated total throughput exceeding 8.9 Tb/s when all beams were active.

Further advancements have explored the use of silicon photonic integrated phased arrays as compact and scalable beam steering devices. Wang et al. [74] designed such a system and achieved 12.5 Gb/s error-free transmission over a 1.4-metre distance using on-off keying (OOK) modulation. These phased arrays offer fast reconfiguration and integration potential, though they often require precise fabrication and calibration.

Despite their performance advantages, beam steering systems face several challenges. The complexity and cost of the optical components—such as tunable lasers, precision lenses, and beamforming modules—can hinder large-scale deployment. More critically, scalability is constrained by the number of tunable laser sources available in the system. Each laser source can typically serve only one user at a time, most practical implementations rely on a single or limited number of lasers to serve the entire network. This architectural limitation significantly restricts the number of users that can be simultaneously supported, making it difficult to scale beam steering systems for dense multi-user environments. Additionally, the latency associated with beam reconfiguration and initial user search pose further limitations in highly dynamic or cluttered indoor settings.

2.2.2 Static grid-of-beams system

In contrast to the dynamic beam steering approach, recent research has explored alternative architectures that eliminate the need for active beam redirection. One such approach is the static grid-of-beams (GOB) method, which relies on a dense, fixed array of narrow beams to provide full coverage of the service area. These systems are designed to maintain continuous connectivity by ensuring that the user device (UD) is within the coverage area of at least one beam, where each beam is associated with its own dedicated active laser source. This architecture avoids the complexity and latency associated with real-time beam steering, offering a more scalable and parallelizable solution for multi-user environments.

A representative example of this paradigm is the beam-domain massive multiple-input multiple-output (MIMO) OWC system proposed by Sun et al [70]. In their design, a large transmit lens is positioned in front of an LED array, refracting light from each element in different directions. This configuration enables a single optical AP to simultaneously serve multiple user terminals across a wide indoor area.

Building on this concept, other works have proposed laser-based IR OWC systems using VCSEL arrays to achieve aggregate data rates exceeding 1 Tb/s [41]. VCSELs are particularly well-suited for GOB architectures due to their high-power efficiency, broad modulation bandwidth, and well-controlled beam profiles. Compared to edge-emitting lasers, VCSELs are easier to fabricate, more reliable, and can be precisely arranged in two-dimensional arrays at low cost [57].

Liu et al [83]. further advanced this approach by designing an optical wireless transmitter system based on a 5×5 VCSEL array, combined with cascaded optical components for beam collimation, homogenization, and expansion. Using micro-lens arrays and planoconvex lenses, they demonstrated uniform beam coverage over a $1 \times 1\ m^2$ area at a 3-metre distance, with each beam spot measuring $20 \times 20\ cm^2$. Experimental results from a linear 1×4 VCSEL array confirmed data rates of 8 Gb/s per beam spot at a pre-forward error correction (FEC) bit error rate (BER) of 3×10^{-3}, with an anticipated aggregate throughput of 200 Gb/s.

To further enhance scalability and simplify deployment, Kazemi et al. [41] propose a double-tier AP architecture, incorporating an array of VCSEL arrays—referred to as an "array of arrays." Each transmitter element in this architecture is composed of a VCSEL array and a plano-convex lens, with a predefined orientation to cover a specific region of the network, as shown in Figure 3.1. This design enables the creation of a dense, static grid of laser beams, offering full spatial coverage without the need for beam steering mechanisms.

For the analysis of handover mechanisms in this thesis, we adopt the array-of-arrays transmitter architecture as the reference system. This choice is motivated by its status as the most comprehensive and recent advancement in the field of NB-OWC, offering a scalable and high-capacity solution for indoor environments. Moreover, the structured layout of this network facilitates a straightforward localization strategy, as detailed in Section 3.3.3, which is essential for accurate user trajectory tracking.

2.3 Hybrid OWC/RF networks

Despite their promising capabilities in delivering ultra-high-speed wireless connectivity, NB-OWC systems inherit and amplify several inherent limitations of optical wireless communication technologies. Chief among these is their strict reliance on LoS transmission. The highly directional nature of narrow beams makes these systems exceptionally sensitive to physical obstructions, which can easily disrupt the communication link and lead to service degradation or complete outages [20].

Moreover, the reduced coverage footprint of each beam presents significant challenges in maintaining continuous connectivity for mobile users. In ultra-dense deployments, users frequently transition between narrowly confined coverage zones, resulting in frequent handovers. This increases the risk of service interruptions, thereby negatively impacting the overall QoS.

The cumulative effect of these limitations underscores the need for novel network configurations and architectural combinations that can mitigate the drawbacks of NB-OWC systems while preserving their advantages. This motivates the exploration of hybrid optical/RF network designs, which aim to leverage the complementary strengths of both technologies to enable robust, seamless, and high-performance wireless communication in complex indoor environments [78].

To address the challenges inherit to pure OWC, hybrid optical/RF wireless networks have emerged as a promising solution. By integrating the high-capacity, interference-free characteristics of OWC with the robustness and mobility support of RF technologies, hybrid architectures aim to deliver seamless

and resilient wireless connectivity [79]. This synergy enables the network to dynamically adapt to changing environmental and user conditions, leveraging the strengths of each technology where they are most effective.

It is important to note, however, that the majority of existing research on hybrid optical/RF systems, especially in the context of indoor networks, has focused on wide-beam Li-Fi configurations—often referred to as Li-Fi 1.0 [30]. In contrast, the integration of NB-OWC systems into hybrid architectures remains largely unexplored. This thesis aims to bridge that gap by investigating how narrow beam systems can be effectively incorporated into hybrid networks, with a particular focus on mobility management.

The concept of hybrid Li-Fi and Wi-Fi networks (HLWNets) was first introduced by Rahaim et al. in 2011 [64], combining the high-speed data transmission capabilities of Li-Fi with the ubiquitous coverage of Wi-Fi. This foundational work was later extended by Stefan et al. [73], who explored the integration of Li-Fi with femtocell networks. These early studies demonstrated that hybrid architectures can outperform standalone Li-Fi or RF systems in terms of overall network performance, particularly in complex indoor environments.

Building on this previous work, this thesis focuses on an evolution of HLWNets that incorporates Li-Fi 2.0 [43] characterized by narrow beam OWC systems—in tandem with Wi-Fi. The NB-OWC system provides significant additional capacity, while the Wi-Fi component complements it by offering enhanced robustness and reliability. This hybrid configuration aims to harness the strengths of both technologies to support high-throughput, low-latency, and mobility-resilient communication in next-generation indoor wireless networks.

2.3.1 Hybrid network topology

In hybrid optical/RF wireless systems, the division of uplink and downlink responsibilities is a critical design consideration that depends on the capabilities of the underlying technologies and the requirements of the target applications [20]. Due to the limited transmission power and hardware constraints of typical optical wireless receivers—such as those found in smartphones—optical wireless communication (OWC) systems, including Li-Fi, are generally not well-suited for uplink transmission [34]. As a result, the uplink in hybrid systems is typically managed by the RF component, which offers greater flexibility and reliability for user-to-network communication.

The downlink, on the other hand, can be handled by either the optical or RF subsystem, depending on the deployment strategy and environmental conditions. According to Feng et al. [25], three primary configurations are commonly considered for downlink communication in hybrid RF/OWC systems:

- **Optical network for downlink:** In this configuration, the downlink is exclusively managed by the OWC system. This approach is straightforward and leverages the high data rate capabilities of Li-Fi. However, it is highly susceptible to misalignment, shadowing, multipath effects, intersymbol interference, and other optical channel impairments, which can compromise link reliability.

- **RF as a backup for optical downlink:** Here, the optical system serves as the primary downlink, while the RF system acts as a fallback. When

the optical link is disrupted—due to blockage or signal degradation—the system seamlessly switches to the RF link to maintain service continuity. Once the optical link is restored, the system reverts to the high-capacity optical channel [78]. This strategy enhances reliability without sacrificing the benefits of high-speed optical transmission.

- **Simultaneous optical and RF downlink** This approach utilizes both optical and RF links concurrently to maximize downlink throughput. While it offers the highest potential capacity, it also introduces significant complexity in terms of traffic management, synchronization, and dynamic load balancing. Advanced algorithms are required to split and coordinate data streams across the two channels effectively [79]. This is a nascent field, with protocols capable of operating across both mediums still to be developed [11]. As such, this strategy is acknowledged but falls outside the scope of this thesis

Building on these established strategies, this thesis explores a hybrid network topology that integrates narrow beam OWC (Li-Fi 2.0) system with Wi-Fi. In this configuration, the NB-OWC system is primarily responsible for delivering high-speed downlink data, while the Wi-Fi system supports uplink communication and provides robustness on the downlink during mobility events. This setup corresponds to the second configuration described above, where RF acts as a backup for the optical downlink. Notably, this configuration aligns with the dominant approach found in the existing literature on HLWNets [80], making it a practical and well-supported foundation for exploration and observation.

2.4 Handover management in hybrid OWC/RF networks

Mobility management is a critical aspect of wireless network design, particularly in environments where users frequently move between coverage zones. In hybrid wireless networks comprising both OWC and RF technologies, mobility management becomes even more complex due to the heterogeneous nature of the underlying systems [20]. One of the central components of mobility management is the handover process, which refers to the process of transferring an active communication session from one access point or technology to another without service interruption [8].

In general, the handover process in hybrid networks can be categorized into two types [79]:

- **Horizontal handover (HHO)**: Occurs within the same wireless access technology (e.g., between two Wi-Fi access points).

- **Vertical handover (VHO)**: Involves switching between different technologies (e.g., from Li-Fi to Wi-Fi), and the air interface changes.

Although efficient VHO schemes have been extensively studied in RF-based heterogeneous networks, the unique characteristics of optical channels, particularly their sensitivity to user movement and LoS conditions, make VHO between

RF and OWC systems significantly more complex than in all-radio environments. These challenges are compounded by differences in the physical and data-link layer mechanisms between optical and RF systems, which complicate mobility management in hybrid networks [33]. While a substantial body of research exists on handover mechanisms for heterogeneous networks (HetNets), including received signal strength (RSS)-based handovers, load balancing techniques, and energy-efficient schemes [52], managing handovers in HLWNetss presents additional difficulties. The small coverage areas of Li-Fi access points lead to more frequent handover events and increased sensitivity to user mobility and environmental dynamics, requiring more adaptive and responsive mobility solutions [79].

Appropriate handover decision criteria and algorithms remain open research questions in the context of optical wireless hybrid networks. Key challenges include accurately estimating channel conditions under mobility, minimizing handover latency, and ensuring seamless transitions between technologies without compromising QoS.

As mentioned in Section 2.3, hybrid networks incorporating NB-OWC systems remain a largely unexplored area in current research. Therefore, the following subsections first examine handover mechanisms developed for pure NB-OWC systems, followed by a review of handover mechanisms employed in existing HLWNets architectures for comparison.

2.4.1 Reactive vs predictive handovers

Handover mechanisms in wireless networks can generally be classified into reactive and predictive approaches, each with distinct operational principles and implications for system performance.

Reactive handovers are initiated based on the observation of real-time measurements collected over a period of time. These measurements typically include metrics such as RSS, SINR, or BER. A handover is triggered either when the current link quality falls below a predefined threshold or when another access point or cell offers significantly better service. While reactive schemes are relatively straightforward to implement and do not require prior knowledge of user behavior, they often suffer from increased latency and a higher risk of service disruption,especially in environments with rapid mobility. In narrow beam optical wireless systems, where link stability is highly sensitive to user orientation and movement, reactive handovers may result in frequent disconnections and degraded QoS.

In contrast, predictive handovers aim to anticipate the need for a handover before the link quality deteriorates to unacceptable levels. These mechanisms leverage contextual and historical information—such as user trajectory, velocity, mobility patterns, or environmental awareness—to forecast future connectivity conditions. By initiating handovers proactively, predictive schemes can reduce latency, avoid unnecessary handovers, and improve overall system performance. This is particularly advantageous in hybrid Li-Fi/RF networks, where the disparity in coverage, channel characteristics, and mobility sensitivity between technologies makes seamless transitions more challenging.

In the context of narrow beam optical wireless systems, the utilization of predictive handover mechanisms represents a promising direction for enhancing mobility management. The following section reviews existing handover mech-

anisms developed specifically for NB-OWC environments, highlighting how predictive techniques have been applied to address the unique challenges posed by highly directional links and limited coverage area.

2.4.2 Handover mechanisms for NB-OWC

Due to the highly directional nature of NB-OWC beams, maintaining a stable link in the presence of user mobility is a significant challenge. The small coverage area of each beam and the strict LoS requirement make NB-OWC systems particularly susceptible to frequent link disruptions. As a result, handover mechanisms in such systems must be both rapid and precise to ensure seamless connectivity.

To date, research on handover mechanisms specifically tailored to NB-OWC remains limited. The only notable contribution in this domain is the work by Pham et al. in [63]. This study presents a comprehensive framework for managing mobility in beam steering based NB-OWC environments, with a focus on minimizing handover latency and ensuring service continuity.

This approach is based on a beam tracking and prediction mechanism that leverages user movement patterns to anticipate the need for handover. The system employs a multi-beam transmitter array and dynamically selects the optimal beam based on the predicted user position. This proactive strategy reduces the likelihood of link loss and minimizes the time required to re-establish communication when a handover occurs.

A key strength of this work lies in its integration of mobility prediction with beam steering, which allows the system to preemptively adjust the beam direction before the user exits the coverage of the current serving beam. Simulation results demonstrate that this method significantly reduces handover frequency and improves overall system throughput compared to reactive handover mechanisms.

However, the study also has several limitations. First, the effectiveness of the prediction model is highly dependent on the accuracy of user movement estimation, which may be affected by erratic or non-linear mobility patterns. Second, the prediction is performed on an instantaneous time-slot basis, rather than over a longer temporal window. This short-term focus makes the system vulnerable to ping-pong effects, where users may rapidly switch between adjacent beams or cells due to transient blockages or minor fluctuations in channel quality. Additionally, the computational overhead associated with real-time beam selection and steering poses scalability challenges, particularly in multi-user scenarios. This is further exacerbated by the tuning delay of the laser, which can limit the responsiveness of the system to fast-changing user positions.

Crucially, the proposed handover mechanism is designed exclusively for horizontal handovers. The mechanism cannot address vertical handovers through its location prediction criteria. As such, while the work provides valuable insights into intra-system mobility management, it cannot be directly extrapolated to hybrid network scenarios where inter-technology transitions are required.

2.4.3 Handover mechanisms for HLWNets

The heterogeneous nature of HLWNets complicates mobility management, particularly handover design. Existing mechanisms often rely on reactive triggers

or computationally intensive predictive models. Both approaches pose challenges for NB-OWC. This section critically reviews current HLWNets handover mechanisms, focusing on their feasibility and limitations in NB-OWC contexts.

A series of works by Wu et al. [[77], [76], [78]] progressively address the handover challenges in HLWNets. The initial proposal introduces a handover skipping (HS) mechanism based on RSS and its rate of change, aiming to reduce frequent handovers without requiring trajectory data. Subsequent work refines this approach by incorporating user speed to adapt network preference, and later by applying machine learning to dynamically balance channel quality, resource availability, and mobility.

While each paper improves throughput and reduces unnecessary handovers, all three approaches share a common limitation: they are fundamentally reactive and rely on traditional hard handover logic. This makes them unsuitable for NB-OWC systems, where the significantly smaller coverage area and directional sensitivity demand proactive, low-latency handover mechanisms. Moreover, the machine learning-based mechanism introduces additional computational overhead, further limiting its feasibility in real-time NB-OWC deployments.

Building on the handover and load balancing mechanisms proposed by Wu et al., Ji et al. [37] introduce attention-based temporal convolutional neural network (A-TCNN), a deep neural network architecture designed to address load balancing in HLWNets with a varying number of users. Unlike conventional methods that require retraining when user numbers change, A-TCNN performs access point selection for individual users based on the conditions of other users, achieving sub-millisecond runtime and outperforming traditional DNNs in throughput. While the reduction in computational complexity marks a significant advancement, the underlying assumptions remain unchanged. The model is tailored to conventional HLWNet architectures and does not account for the spatial granularity and frequent horizontal handovers inherent in NB-OWC systems, limiting its applicability in such environments.

A pair of studies by Ma et al. [56, 55] propose increasingly sophisticated handover mechanisms for HLWNets. The first introduces a strategy that classifies handover events into three categories and computes optimal dwell times using multiple attributes such as channel quality, user velocity, and data arrival rate. The second builds on this by applying an unsupervised learning-based approach aimed at reducing complexity while improving performance in 6G internet of things (IoT) scenarios. Both methods demonstrate strong gains in throughput, frequency of handovers, and delay. However, they share a key limitation: both assume a simplified network model with a single optical beam and RF access point, focusing exclusively on vertical handovers. This abstraction fails to capture the horizontal handover dynamics critical to NB-OWC systems, where ultra-small beam coverage demands high spatial resolution and frequent intra-technology transitions. As such, these mechanisms lack the granularity and responsiveness required for effective mobility management in narrow beam environments.

Odabaşı et al. [60] propose a predictive vertical handover algorithm for HLWNets that uses a machine learning-based forecasting model to anticipate Li-Fi link blockages caused by human movement. By predicting the duration of upcoming blockages, the algorithm proactively switches between Li-Fi and Wi-Fi to balance average available data rate (AADR) and minimize service interruptions. While the approach demonstrates strong performance in simulated envir-

Table 2.2: **Comparison of Existing Handover Mechanisms in HLWNet and NB-OWC Systems**

Method	HHO	VHO	Type	Limitations
Pham et al. [63]	✓		Predictive	Only supports HHO; short-term prediction; high overhead; not suitable for hybrid networks
Wu et al. [[77]-[78]]	✓	✓	Reactive	Not suitable for NB-OWC; lacks spatial granularity;
Ji et al. [37]	✓	✓	Predictive	Not designed for NB-OWC; lacks support for frequent HHO
Ma et al. [55], [56]		✓	Predictive	Simplified model; ignores HHO; lacks responsiveness
Odabaşı et al. [60]		✓	Predictive	Only supports VHO; coarse model; online-ML model adds latency

onments, it focuses solely on vertical handovers and assumes a coarse-grained network model. This limits its applicability to NB-OWC systems, where horizontal handovers dominate due to ultra-small beam coverage. Additionally, the reliance on online machine learning models, which update parameters incrementally as new data arrives, introduces latency and computational overhead, making them less suitable for the fast, fine-grained handover decisions required in narrow beam scenarios.

Despite notable advancements in handover mechanisms for hybrid Li-Fi-Wi-Fi networks, existing approaches consistently fall short when applied to hybrid NB-OWC/RF systems. Most mechanisms rely on reactive decision-making or coarse-grained vertical handover models, assuming broad coverage from a single optical and RF access point. This abstraction neglects the horizontal handover complexity introduced by NB-OWC's ultra-small beam coverage, where frequent intra-technology transitions are inevitable. Even predictive schemes leveraging machine learning suffer from high computational overhead and lack the spatial granularity required for real-time responsiveness. Notably, the only handover mechanism specifically tailored for NB-OWC focuses solely on horizontal handovers and exhibits significant limitations in adaptability and scalability, particularly within hybrid network contexts. Consequently, there remains a clear research gap: the need for lightweight, predictive handover mechanisms specifically designed for NB-OWC within hybrid architectures, capable of handling fine-grained mobility.

To summarize the limitations and characteristics of existing handover mechanisms in HLWNet and NB-OWC systems, Table 2.2 provides a comparative overview.

Chapter 3

System model

This chapter elaborates on the modelling aspects of the system being simulated. Having accurate models for both RF and Optical channels is essential for ensuring the reliability and performance of the simulation. These models provide a foundation for understanding and optimizing the system's behaviour under various conditions.

3.1 Network model

In this thesis, we consider an indoor hybrid network comprising a RF network and a NB-OWC network operating in parallel. At any given time, the user equipment (UE) is connected to only one of these networks. A VHO is triggered by the network management system when a switch between networks is deemed necessary.

Each network is modeled with a single AP located at the center of the simulation space. To isolate and analyze the handover mechanism, we adopt a single-user scenario, as handover decisions are made independently for each user. The user begins at a randomly selected position on the receiver plane and moves throughout the simulation period according to the mobility model described in Section 3.3.1.

The UE is assumed to be equipped with appropriate receivers for both the RF and NB-OWC networks, as detailed in Subsections 3.1.1 and 3.1.2, .

3.1.1 Wi-Fi network model

A single isotropic Wi-Fi AP is positioned at the center of the room, aligned with the receiver plane at ground level. This AP provides full coverage across the entire simulation area. UE is equipped with a single-antenna receiver for RF communication.

3.1.2 Optical network model

The optical network consists of a single AP located at the center of the simulation area, mounted at a fixed height of $h_{DL} = 3\,\text{m}$. The AP follows the "array-of-arrays" architecture proposed in [67] and [41]. This double-tier design

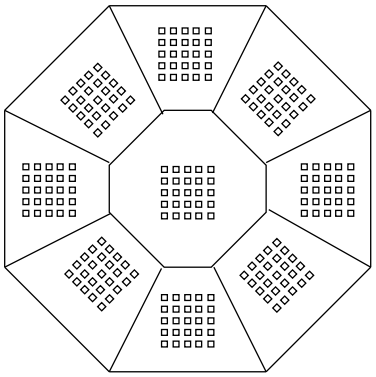

Figure 3.1: **Double-tier access point architecture using array of arrays of VCSELs (top view). This design involves nine 5 × 5 VCSEL arrays**

organizes VCSELs into multiple matrix structures. These matrices are strategically positioned and oriented to ensure complete optical coverage across the entire simulation area.

Figure 3.1 shows the top view of the two-tier AP design, while Figure 3.2 illustrates the resulting network coverage and the association between VCSELs and cells. The AP consists of $N_{VCSEL} = 225$ VCSELs, arranged across 9 transmitter elements in a 3×3 grid, with each element containing $5 \times 5 = 25$ VCSELs. Each VCSEL emits a single optical beam, providing coverage to a small portion of the receiver plane. Lenses are positioned in front of each element to separate the beam spots on the receiver plane and minimise overlap.

The receiver on the UE employs a PD matrix comprising 25 equidistant PDs for optical signal detection. While this approach simplifies the system design, it constrains the UE to a fixed upward-facing orientation to maintain consistent coverage. To overcome this limitation, Sarbazi et al. [66] propose a novel angle diversity receiver (ADR) module mounted atop the PD matrix, consisting of seven compound parabolic concentrators (CPC)s. These CPCs introduce angle diversity, enabling the UE to sustain reliable connectivity even when its orientation varies.

However, to manage simulation complexity, we adopt a simplified receiver model that utilises only the PD matrix, with a total active detection area of $A_{PD} = 2\,\mathrm{cm}^2$, as proposed in [67].

3.2 Channel model

3.2.1 Wi-Fi channel model

Channel gain

The channel gain between the UE and the Wi-Fi AP, denoted by $G^u_{\text{Wi-Fi}}$, incorporates the effects of small-scale fading, path loss, and shadowing. It is

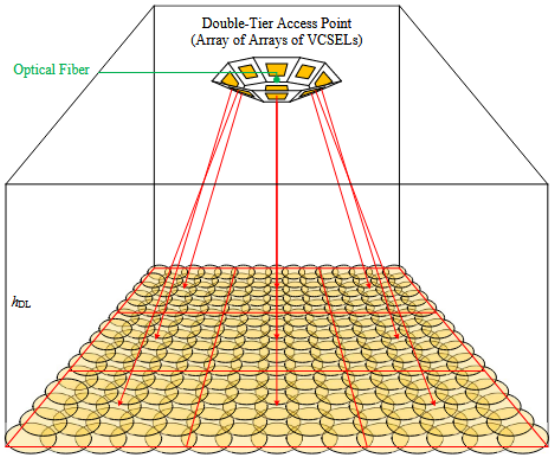

Figure 3.2: **Indoor grid-of-beam optical wireless multi-user access network using the proposed double-tier AP design based on an array of arrays of VCSELs [41]**

computed as

$$G^u_{\text{Wi-Fi}} = |H^u_{\text{Wi-Fi}}|^2 \cdot 10^{\frac{-L(d_u)+X_\sigma}{10}}, \tag{3.1}$$

where $H^u_{\text{Wi-Fi}}$ represents the channel transfer function as described by (3.2), X_σ denotes the shadow fading modelled as a Gaussian random variable, and $L(d_u)$ corresponds to the free-space path loss experienced over a distance d_u [62].

Channel transfer function

The channel transfer function for the Wi-Fi channel, denoted $H^u_{\text{Wi-Fi}}$, follows a standard Rayleigh fading model. Its probability density function (PDF) is given by

$$f(x;\sigma) = \frac{x}{\sigma^2} \exp\left(-\frac{x^2}{2\sigma^2}\right), \quad x \geq 0, \tag{3.2}$$

where the standard deviation σ is equal to 1.

Shadow fading

Shadow fading for the Wi-Fi channel is modelled as a Gaussian random variable, denoted X_σ. Its PDF is defined as

$$f(x) = \frac{1}{\sqrt{2\pi\sigma^2}} \exp\left(-\frac{(x-\mu)^2}{2\sigma^2}\right), \tag{3.3}$$

where the mean is $\mu = 0$ and the standard deviation is $\sigma = 10\,\text{dB}$.

Free-space path loss

The free-space path loss for the Wi-Fi channel, denoted $L(d)$, is defined piecewise as [75]

$$L(d) = \begin{cases} 20\log_{10}(f_c d) - 147.5, & \text{if } d < d_{\text{ref}}, \\ 20\log_{10}\left(f_c \frac{d^{2.75}}{d_{\text{ref}}^{1.75}}\right) - 147.5, & \text{if } d \geq d_{\text{ref}}, \end{cases} \tag{3.4}$$

where f_c represents the central carrier frequency, and $d_{\text{ref}} = 10\,\text{m}$ is the reference distance.

3.2.2 Optical channel model

Beam propagation

The laser beam emitted by the VCSEL is assumed to exhibit a Gaussian intensity profile. It is characterised by the beam waist w_0 and the wavelength λ, and propagates along the z-axis, with the beam waist located at the origin. The intensity distribution is described by

$$I(r, z) = \frac{2P_t}{\pi w^2(z)} \exp\left(-\frac{2r^2}{w^2(z)}\right), \tag{3.5}$$

where P_t is the transmitted optical power, r and z denote the radial and axial positions respectively, and $w(z)$ is the beam radius at a distance z [65].

The beam radius $w(z)$ evolves with propagation distance according to

$$w(z) = w_0\sqrt{1 + \left(\frac{z}{z_R}\right)^2}, \tag{3.6}$$

where z_R denotes the Rayleigh range, defined as

$$z_R = \frac{\pi w_0^2 n}{\lambda}, \tag{3.7}$$

and n is the refractive index of the medium. The Gaussian beam may also be characterised using the complex beam parameter $q(z)$, given by

$$q(z) = z + jz_R, \tag{3.8}$$

which combines the beam's propagation distance and Rayleigh range.

Lens transformation

When a Gaussian beam passes through a lens, it is transformed into another Gaussian beam with modified parameters. The resulting beam is characterised by a new beam waist w_0', Rayleigh range z_R', and complex beam parameter q'. The relationship between the input and output beam parameters in an optical system can be described using the ABCD matrix formalism [65].

For Gaussian beams, the ABCD law applies specifically to the complex beam parameter q, relating the input parameter q to the output parameter q' through the transformation

$$q' = \frac{Aq + B}{Cq + D}, \tag{3.9}$$

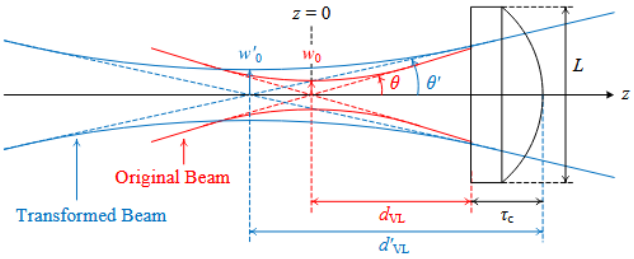

Figure 3.3: **Transformation of a Gaussian beam by a plano-convex lens, showing a virtual image of the beam waist behind the lens [41].**

which is applicable to any paraxial optical system represented by an ABCD matrix.

In the case of a plano-convex lens, the corresponding ABCD matrix is determined by the lens thickness τ, the radius of curvature R_{lens}, and the refractive index n_{lens}. The parameters are given by

$$A = 1, \tag{3.10a}$$

$$B = \frac{\tau}{n_{\text{lens}}}, \tag{3.10b}$$

$$C = \frac{1 - n_{\text{lens}}}{R_{\text{lens}}}, \tag{3.10c}$$

$$D = 1 + \frac{\tau}{R_{\text{lens}}} \left(\frac{1}{n_{\text{lens}} - 1} \right), \tag{3.10d}$$

as described in [32].

The beam transformation is first applied between the original beam at $z = d_{VL}$, where d_{VL} is the distance between a VCSEL and the lens, and the transformed beam at $z = d_{VL} + \tau$ (i.e., at $z' = d'_{VL}$), as illustrated in Figure 3.3. This results in the complex beam parameter q' being updated according to

$$q'(d'_{VL}) = d'_{VL} + jz'_R = \frac{A(d_{VL} + jz_R) + B}{C(d_{VL} + jz_R) + D}, \tag{3.11}$$

as shown in [41]. From this updated q' parameter, the corresponding values of w'_0 and z'_R are derived using expressions provided in the same reference.

Optical OFDM

To achieve high data rates in OWC systems, we utilise optical orthogonal frequency division multiplexing (OFDM) techniques, specifically DC-biased optical (DCO)-OFDM, which is widely considered the most bandwidth-efficient variant [67]. DCO-OFDM operates by shifting the envelope of the time-domain signal using a DC bias to satisfy the non-negativity constraint of IM-DD channels. Each VCSEL is assumed to be individually driven by a DCO-OFDM waveform, transmitting an independent data stream to the user within its coverage spot.

The instantaneous optical power emitted by the i^{th} VCSEL at time sample t, where $t = 0, 1, \ldots, N-1$, is given by

$$x_i(t) = \sqrt{P_i} s_i(t) + x_{DC}, \tag{3.12}$$

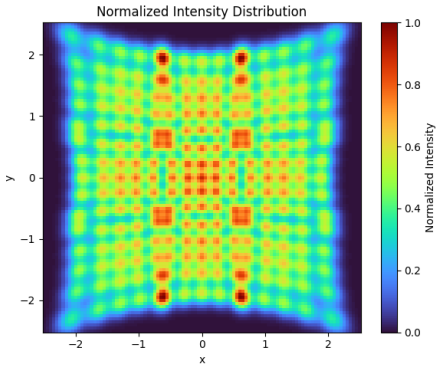

Figure 3.4: **Normalized intensity distribution of the double-tier AP on the receiver plane**

where P_i is the average electrical power of the OFDM symbol, $s_i(t)$ is the normalised discrete-time OFDM signal, and x_{DC} is the DC bias, equal to the transmission power P_t.

The average electrical power of VCSEL$_i$, for $i = 1, 2, \ldots, N_{\text{VCSEL}}$, is defined as

$$P_i = \frac{1}{9} P_t^2, \tag{3.13}$$

where P_t denotes the transmission power of the VCSEL.

Total spatial intensity

After lens transformation, the total spatial intensity of the AP at a point $P = (x, y)$ on the receiver plane is computed as

$$\text{IAP}(x, y) = \sum_{i=1}^{225} \frac{2P_t}{\pi w'^2(d_v \cos\phi_i)} \exp\left(-\frac{2d_v^2 \sin^2\phi_i}{w'^2(d_v \cos\phi_i)}\right), \tag{3.14}$$

where P_t is the transmission power of the VCSEL, $w'(\cdot)$ is the post-lens beam radius as defined in (3.6), d_v is the Euclidean distance between the transmitter and point P, and ϕ_i is the radiance angle of the beam emitted by VCSEL$_i$ with respect to P.

Figure 3.4 illustrates the normalised intensity distribution across the simulation space[1].

[1]Deviations were observed in the shape of the normalised intensity distribution compared to those presented in [41]. These deviations affect the overall distribution generated by the optical access point but do not impact the fundamental behaviour of the individual Gaussian beams. Crucially, they do not influence the performance evaluation of the handover mechanism, as this study is comparative in nature, benchmarking against a baseline approach. For further discussion of the differences and the validation tests performed to verify the correctness of the implementation, see Appendix A.

DC channel gain

The received photocurrent at the receiver on the UE from VCSEL_i is given by

$$y(t) = R_{\text{PD}} h_i x_i(t) + \sum_{j \neq i} R_{\text{PD}} h_j x_j(t) + v(t), \tag{3.15}$$

where the PD responsivity is denoted by R_{PD}, and $v(t)$ represents the additive white gaussian noise (AWGN), which comprises thermal noise, shot noise from the receiver, and the relative intensity noise (RIN) of the VCSEL.

In (3.5), h_j represents the direct current (DC) channel gain between the receiver located at (x, y) and VCSEL_j at position (a_j, b_j), and is given by

$$h_j = \iint_{\mathcal{A}_{\text{PD}}} \frac{2}{\pi w^2(z)} \exp\left[-2\frac{(x-a_j)^2 + (y-b_j)^2}{w^2(z)}\right] dx\, dy, \tag{3.16}$$

where $\mathcal{A}_{PD}$ denotes the set of points on the xy-plane with the desired PD located at the origin, encompassing the entire area of the photodetector in question. The cardinality of this set is given by $|\mathcal{A}_{PD}| = A_{PD}$, where A_{PD} represents the total area of the PD matrix and $|\cdot|$ denotes the cardinality of the set.

Thermal noise

Thermal noise is an intrinsic noise source in wireless optical systems caused by the random motion of electrons due to temperature, and its variance is given by

$$\sigma^2_{\text{thermal}} = \frac{4kT}{R_L} B F_n, \tag{3.17}$$

where k is the Boltzmann constant, T is the temperature in kelvin, R_L is the load resistance, F_n is the noise figure of the transimpedance amplifier (TIA), and B is the bandwidth of the VCSEL.

Shot noise of the receiver

Shot noise in optical wireless networks is a type of noise generated by the quantum nature of light, where the discrete nature of photons causes random fluctuations in the photocurrent at the receiver [66]. The variance of the shot noise at the receiver is given by

$$\sigma^2_{\text{shot-noise}} = 2q_e \left(\sum_{j=1}^{N_{VCSEL}} R_{PD} h_j P_t \right) B, \tag{3.18}$$

where R_{PD} is the responsivity of the photodetector, q_e is the elementary charge, h_j is the DC channel gain given by (3.16), P_t is the transmit power of the VCSEL, and B is the bandwidth of the VCSEL.

Relative intensity noise

RIN refers to the fluctuations in the optical power of a laser, normalised to its average value. The variance of RIN is given by

$$\sigma^2_{\text{RIN}} = \text{RIN} \left(\sum_{j=1}^{N_{VCSEL}} (R_{PD} h_j P_t)^2 \right) B, \tag{3.19}$$

where RIN is the laser noise power spectral density (PSD).

Combining thermal noise, shot noise, and relative intensity noise, the total noise variance of the system is given by

$$\begin{aligned}\sigma^2 &= \sigma^2_{\text{thermal}} + \sigma^2_{\text{shot-noise}} + \sigma^2_{\text{RIN}} \\ &= \frac{4kT}{R_L} BF_n + 2q_e \left(\sum_{j=1}^{N_{VCSEL}} R_{PD} h_j P_t \right) B + \text{RIN} \left(\sum_{j=1}^{N_{VCSEL}} (R_{PD} h_j P_t)^2 \right) B.\end{aligned} \tag{3.20}$$

3.2.3 Wi-Fi performance evaluation

SNR

Based on the Wi-Fi channel model described in Section 3.2.1, the SNR for the Wi-Fi user is given by

$$\gamma^u_{\text{Wi-Fi}} = \frac{G^u_{\text{Wi-Fi}} P_{\text{Wi-Fi}}}{N_{\text{Wi-Fi}} B_{\text{Wi-Fi}}}, \tag{3.21}$$

where the PSD of the noise at the receiver is represented by $N_{\text{Wi-Fi}}$, while $B_{\text{Wi-Fi}}$ and $P_{\text{Wi-Fi}}$ represent the system bandwidth and the transmit power of the Wi-Fi AP, respectively.

Throughput

Given the SNR, and utilising the Shannon capacity as shown in [77], the throughput is calculated as

$$r_u = \zeta B \log_2(1 + \gamma^u_{Wi-Fi}), \tag{3.22}$$

where ζ is the effective utilisation of the capacity, which is impacted by the various overheads associated with transmission [35].

3.2.4 Optical performance evaluation

SINR

Assuming that all AP VCSELs are active, the SINR is calculated as

$$\gamma_i = \frac{R^2_{PD} h_i^2 P_i}{\sum_{j \neq i} R^2_{PD} h_j^2 P_j + \sigma^2}, \tag{3.23}$$

where R_{PD} represents the responsivity of the PD, h_i denotes the channel DC gain between the i^{th} VCSEL and the user, P_i is the average electrical power as defined in (3.13), and σ^2 is the total noise variance of the system as given in (3.20) [67].

Throughput

Based on the work in [67], the reliable transmission rate for each VCSEL is determined from the BER performance. For the channel described in Section 3.2.2, a tight upper bound for the BER—accurate within 1 dB for $M \geq 4$ and $0 \leq \gamma_i \leq 30$ dB—is given by

$$\text{BER} \leq 0.2 \exp\left(\frac{1.5\gamma_i}{M-1} \right), \tag{3.24}$$

where M is the QAM constellation size and γ_i is the SINR of VCSEL$_i$ as defined in (3.23) [28].

The highest order of the QAM constellation, denoted by M_i, is obtained by solving (3.24) with equality for M_i, and is expressed as

$$M_i = 1 + \frac{\gamma_i}{\Gamma}, \tag{3.25}$$

where Γ models the SINR gap, defined by

$$\Gamma = \frac{-\ln(5\text{BER})}{1.5}, \tag{3.26}$$

as specified by the FEC limit [67].

The throughput of VCSEL$_i$ is then given by

$$r_i = \zeta B \log_2 M_i, \tag{3.27}$$

where B is the VCSEL bandwidth, $\zeta = \frac{N-2}{N}$ is the effective utilisation factor, and N is the number of sub-carriers in DCO-OFDM as described in Section 3.2.2.

3.3 User model

3.3.1 User mobility model

User mobility is commonly modelled using popular stochastic frameworks such as the Manhattan mobility model, the reference point group mobility model [40], and the random waypoint (RWP) model [38]. Among these, the RWP model is widely employed in studies of mobile ad hoc networks (MANETs) to simulate mobile node movement patterns. In this model, each node pauses for a random duration at a given location before selecting a new random destination within the simulation area. The node then travels towards this destination at a speed uniformly distributed between predefined minimum and maximum values. Upon arrival, the node pauses again before repeating the process. This thesis adopts the RWP model owing to its simplicity and flexibility in generating diverse mobility patterns.

Originally, the RWP was designed for large outdoor scenarios, featuring varying speeds when arriving at each waypoint. When adapting the model for indoor environments, as done by [78], where distances between waypoints are shorter, the speed is assumed to remain constant over a short interval. This interval is referred to as an *excursion*. At the end of each excursion, the user selects a new speed independently of prior movements and continues travelling. Let v denote the average speed; the user's speed is assumed to be uniformly distributed between 0 and $2v$. Figure 3.5 illustrates an example user movement trace generated by the RWP model in the simulator.

3.3.2 User localisation

User localisation is an essential prerequisite for a mobility-aware handover algorithm to operate effectively. The localisation strategy varies depending on the receiver and transmitter designs as well as the components used within the hybrid network. However, the handover algorithm itself is not intrinsically

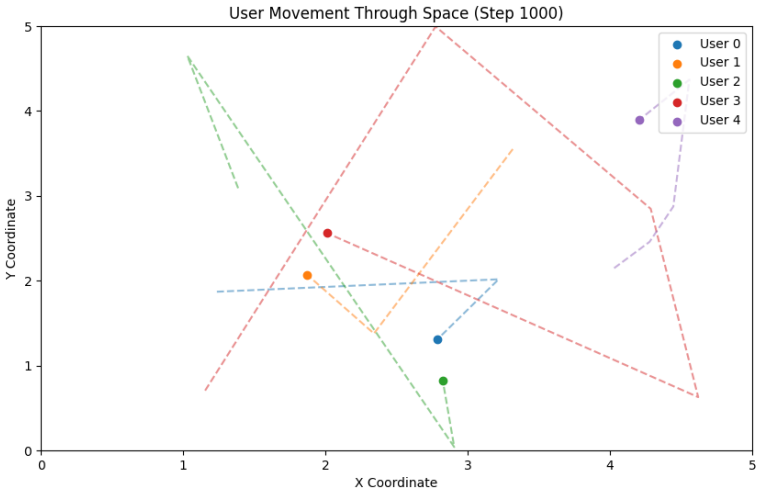

Figure 3.5: **User mobility simulation based on the RWP**

coupled to any specific localisation method. It treats localisation as a black box, extracting only the data necessary for its decision-making process.

Consequently, the handover algorithm can function with any localisation technique that meets the following criteria:

- **Location accuracy:** The localisation method should provide sufficiently accurate positional information relative to the coverage area of an individual optical beam. The goal is for the location estimate to be precise enough for the algorithm to identify the specific optical beam that can serve the user. For instance, in our case, considering the transmitter design, where the coverage area of a single optical beam is less than 10 cm, the localisation strategy should achieve centimetre-level accuracy.

- **Measurement periodicity:** As further discussed in Chapter 4, the algorithm requires velocity and acceleration data to inform its decisions. If these quantities are derived from the localisation system, it is crucial that the location estimates are updated frequently enough to ensure their accuracy and relevance.

Taking into account both the transmitter–receiver design and the requirements of the handover algorithm, we decided to employ a passive beam selection-based strategy, initially proposed in [84]. The beam selection system utilising corner cube retroreflector (CCR) offers low power consumption and negligible delay, enabling real-time tracking for high-speed users.

3.3.3 Localisation based on passive beam selection

The VCSEL array system proposed by Zeng et al. [84] employs a RSS strategy, which selects the optical beams exhibiting the highest received power. Each beam illuminates a distinct region on the receiver plane. By identifying the

three beams with the strongest received power, the system can estimate the user's location via triangulation.

The selection of beam indices used for localisation is formalised as

$$\{I_1, I_2, I_3\} = \arg\max_{n \in N} \{P_n\}_{\text{top } 3}, \tag{3.28}$$

where I_i denotes the index of the selected optical beam, N is the full set of beams, and P_n is the received optical power from the n-th beam.

Localisation is facilitated by the fact that the beam centres of all optical beams are precomputed and stored in a static lookup table. Once the three strongest beams are identified, their known spatial centres can be used to geometrically estimate the user's position via triangulation. The estimated coordinates are given by

$$x = \frac{P_{I_1} x_1 + P_{I_2} x_2 + P_{I_3} x_3}{P_{I_1} + P_{I_2} + P_{I_3}}, \quad y = \frac{P_{I_1} y_1 + P_{I_2} y_2 + P_{I_3} y_3}{P_{I_1} + P_{I_2} + P_{I_3}}, \tag{3.29}$$

where P_{I_i} represents the received optical power from the beam indexed by I_i, and (x_i, y_i) denotes the centre coordinates of beam I_i on the receiver plane.

In summary, the models developed and analysed in this chapter provide a robust framework for understanding the underlying dynamics of the system, laying a solid foundation for the subsequent experimental validation and practical applications discussed in the following chapters.

Chapter 4

Mechanisms to optimize mobility management

This chapter outlines the design and key considerations of the proposed mechanisms developed to address the problem of optimal mobility management in narrow beam systems. The overall strategy is user-centric, operating independently for each user and aiming to maximise throughput based on the user's speed.

We present four mechanisms in this section. The first serves as a baseline for comparison and is drawn from existing literature, specifically Wu et al. [77]. The second mechanism introduces modifications to this reactive method in order to enhance performance. The third and fourth mechanisms are based on a distinct design principle, leveraging prediction based on user location estimation to improve mobility management.

4.1 High-level overview

Before delving into the inner workings of the mechanisms, we first present a high-level overview of the overall handover strategy, specifying the system's inputs and outputs.

We describe four distinct mechanisms, categorised into two overarching mechanisms:

- **Reactive mechanisms:**
  - **Mechanism 1 (Reactive SINR):** A reference method taken from Wu et al. [77], serving as a baseline for comparison. It relies on real-time SINR measurements to make handover decisions.
  - **Mechanism 2 (Reactive throughput):** A modified version of Mechanism 1 that replaces SINR with throughput as the primary measurement metric. Handover decisions are based on observed throughput over multiple time slots.
- **Predictive mechanisms:**

- **Mechanism 3 (Predictive SINR):** A prediction-based method that estimates the user's location a fixed number of time steps into the future. At each predicted location, the corresponding SINR is estimated. Based on this series of future SINR values, a handover decision is made at the end of the prediction horizon.
- **Mechanism 4 (Predictive throughput):** A variant of Mechanism 3 that replaces SINR with predicted throughput as the decision-making metric. Throughput is estimated at each future location, and the handover decision is taken based on the predicted throughput values.

The key distinction lies in the decision-making approach: reactive mechanisms operate on real-time measurements, whereas predictive mechanisms leverage estimated future user locations to proactively execute handovers.

4.2 Inputs and Outputs of the mechanisms

4.2.1 Inputs

The input set varies depending on whether the mechanism belongs to the reactive or predictive category. We categorise the inputs as follows:

Inputs common to both reactive and predictive mechanisms:

- **Current Serving AP/Beam:** The NB-OWC beam or RF AP currently serving the UE when the handover procedure is triggered.
- **RSS Report:** An array containing the RSS measurements recorded by the user for all detectable NB-OWC beams and the RF AP.

Inputs exclusive to predictive mechanisms:

- **User Position:** The coordinates of the UE, obtained using the localisation method described in Section 3.3.3.
- **User Velocity:** Estimated by the UE based on changes in position over time.
- **User Acceleration:** Derived from variations in velocity. It is used in conjunction with position and velocity to improve the accuracy of user trajectory prediction.

4.2.2 Outputs

The output remains consistent across all mechanisms:

- **Choice:** The selected beam/AP (NB-OWC or RF) to which the user should be handed over to.

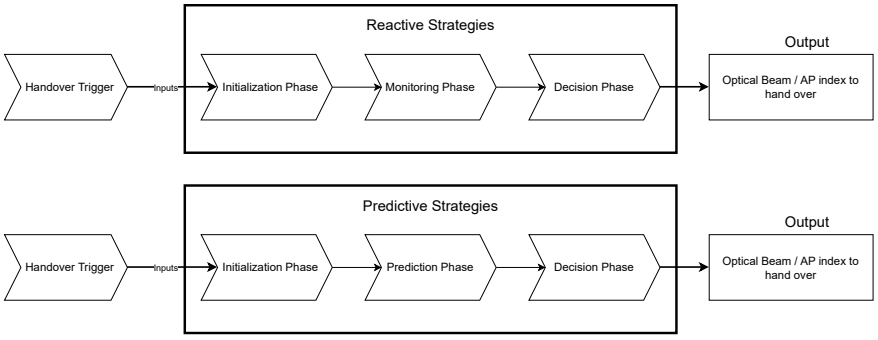

Figure 4.1: **Overview of phases of the mechanisms following reactive and predictive mechanisms**

4.3 Components of the mechanism

The internal operations of each mechanism can be divided into distinct phases. The handover trigger and the initial phase are common to both reactive and predictive mechanisms. The subsequent phases differ depending on the mechanism strategy. Figure 4.1 illustrates a graphical overview of the framework for each of the mechanisms.

4.3.1 Handover trigger

This phase defines the preconditions required for initiating a handover. It also involves the extraction or derivation of the necessary inputs from the UE, including:

- Current serving NB-OWC beam or RF AP
- RSS measurements for all detectable beams and access points
- (For predictive mechanisms only) User position, velocity, and acceleration

4.3.2 Reactive mechanisms

Reactive mechanisms rely on real-time measurements and do not incorporate prediction. The mechanism proceeds through the following phases:

- **Monitoring Phase:** The mechanism monitors the RSS values reported by the UE over multiple consecutive time steps. A handover is considered only if an alternative beam or RF AP consistently provides superior performance across all monitored steps.
- **Decision Phase:** Once a candidate beam or access point has demonstrated consistently better performance, the mechanism selects the one offering the highest SINR or throughput at the current time slot and initiates the handover.

4.3.3 Predictive mechanisms

Predictive mechanisms incorporate user trajectory estimation to proactively determine the best handover target. The mechanism operates in the following phases:

- **Initialisation Phase:** Sets up parameters that govern the behaviour of the mechanism during the current run. Additionally, it initialises specific variables required for trajectory prediction and performance evaluation.
- **Prediction Phase:** Executes operations at each time step within the prediction window. The UE's future positions are estimated using its current motion parameters. At each predicted location, the corresponding SINR or throughput is estimated. These predicted values are then used to assess the suitability of all available NB-OWC beams and RF APs for connection.
- **Decision Phase:** Evaluates the cumulative scores assigned to each NB-OWC beam and RF AP. Based on these scores, a final decision is made regarding the optimal connection target for the UE.

4.4 Handover trigger

All the handover mechanisms follow a trigger-based strategy, meaning that the handover process is initiated only when specific events occur or predefined conditions are met. In this case, the trigger is activated when RSS measurements reported by the UE indicate that a non-serving NB-OWC beam or RF AP is providing a higher SINR/throughput than the current serving beam or access point.

Both the NB-OWC and RF networks periodically transmit reference signals, which are used to compute the RSS measurements. In the NB-OWC network, these reference signals also enable user localisation as elaborated in Section 3.3.3. As the reference signals are transmitted at regular intervals, changes in the user's location between consecutive measurements can be used to estimate velocity.

The UE sends the collected RSS measurements back to the network in the form of an RSS report. The network then uses this report to derive the most up-to-date estimates of the user's location, velocity, and acceleration. Based on these values, the network determines whether the conditions for initiating a handover have been satisfied.

Figure 4.2 provides a graphical illustration of the handover trigger process.

The handover trigger mechanism is consistent across both reactive and predictive mechanisms.

4.5 Parameters of the mechanism

We begin by setting up key parameters that characterise a specific instance of the handover mechanism. These parameters collectively influence and define the behaviour of the selection logic:

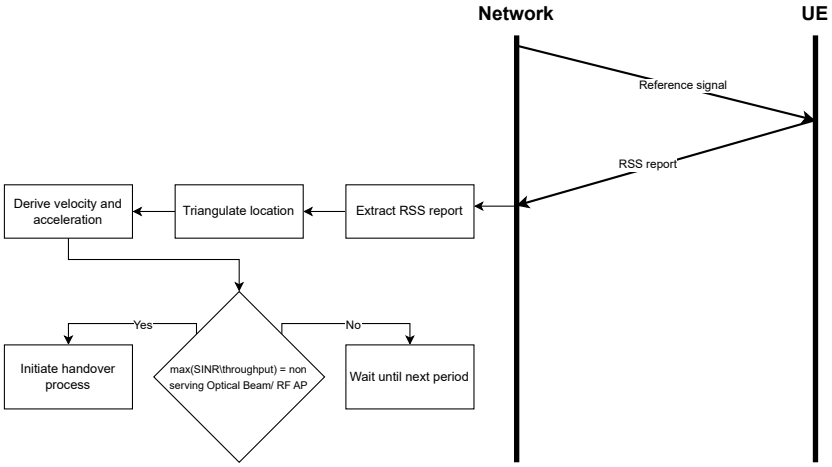

Figure 4.2: **Flowchart describing the handover trigger process**

- **Network Selection Coefficient λ:** This parameter originates from the work of Wu et al. [77], and is based on the assumption that at higher user velocities, the OWC network may struggle to maintain consistent connectivity. In such cases, the mechanism may favour a handover to the RF network. This preference is modelled using the network selection coefficient, λ, a scalar value that reflects the system's inclination towards the RF network. The value of λ increases with user velocity.

  However, the original formulation was developed for HLWNets environments, where both Wi-Fi and Li-Fi networks offer throughput of a similar magnitude (in the order of Mb/s). When applied to systems incorporating NB-OWC, this assumption no longer holds, as there exists a distinct magnitude difference, with NB-OWC offering throughput in the order of Gb/s, compared to Mb/s for Wi-Fi. Consequently, the relationship between λ and user velocity must be re-evaluated to reflect this disparity. The results of λ optimisation are presented in Chapter 5.

- **Prediction Window Size η:** The prediction window size, η, determines how far into the future the mechanism performs estimations before making a handover decision. Its value is governed by the reliability of trajectory prediction. Thus, how many steps ahead the mechanism can safely forecast the user's position with minimal deviation from ground truth.

  At lower speeds, the user covers a smaller distance during each time slot, making their trajectory more stable and predictable. This allows the movement to be approximated as a sequence of short, nearly linear segments, which improves prediction accuracy and thus allows for a larger prediction window. In contrast, at higher speeds, deviations between predicted and actual positions accumulate more quickly, requiring a shorter prediction horizon. Consequently, the acceptable value of η decreases as user velocity increases.

Table 4.1: **Summary of differences between handover mechanisms**

Mechanism	**Strategy**	**Metric**	**Parameters**	
			Lambda	*Eta*
Mechanism 1	Reactive	SINR	✓	×
Mechanism 2	Reactive	Throughput	×	×
Mechanism 3	Predictive	SINR	✓	✓
Mechanism 4	Predictive	Throughput	×	✓

The distribution of these parameters across the mechanisms is as follows:

- **Network Selection Coefficient λ:** Utilised by Mechanisms 1 and 3, which are based on SINR measurements. These mechanisms require λ to model the system's preference for RF connectivity at certain user velocities. In contrast, Mechanisms 2 and 4 are based on throughput measurements and aim to directly optimise for maximum throughput. As such, they do not require λ.

- **Prediction Window Size η:** Required by Mechanisms 3 and 4, which are predictive mechanisms. These mechanisms estimate future user positions and evaluate performance metrics over a prediction horizon. The window size η determines how far into the future these predictions are made. Mechanisms 1 and 2 are reactive mechanisms and operate solely on real-time measurements, thus do not require η.

Table 4.1 provides a summary of the distinct differences between the 4 mechanisms.

4.6 Reactive mechanisms

Two reactive mechanisms are presented. Mechanism 1 uses SINR as the decision metric, while Mechanism 2 employs throughput. Mechanism 1 acts as the baseline for evaluating the performance improvements offered by the predictive mechanisms described in the subsequent section.

Each reactive mechanism follows a three-phase structure: initialisation, monitoring, and decision. The initialisation phase sets up key variables and parameters required for the current execution of the mechanism. The monitoring phase evaluates the performance of available beams and access points over multiple consecutive time slots. A handover is performed only if an alternative consistently outperforms the current connection. Finally, the decision phase selects the optimal beam or AP based on the most recent measurements.

4.6.1 Mechanism 1: Reactive SINR

Initialisation phase

When a handover condition is triggered, the mechanism begins by initialising the following variables:

1. **Dwell Time t_{dwell}:** Specifies the duration for which the monitoring phase must run. During this period, a handover is only considered if another beam or RF AP consistently provides better SINR than the current serving one. A longer dwell time allows for more measurements, reducing the likelihood of the **ping-pong effect**, a phenomenon where the user is handed over repeatedly between access points due to transient fluctuations in signal quality. However, longer dwell times may delay necessary handovers, potentially disrupting service. Conversely, shorter dwell times enable quicker handovers but increase sensitivity to short-term variations, raising the risk of ping-pong behaviour.

2. **Elapsed Time t_{elapsed}:** Tracks the time elapsed since the start of the monitoring phase. It is incremented at each time step, provided that **any** alternative beam or RF AP offers better SINR than the current connection. This condition does not require the same beam or AP to outperform consistently throughout the phase. The variable is initialised to zero.

3. **Prediction Step Size t_{TTT}:** Defines the time interval between consecutive measurements. It determines the increment applied to t_{elapsed} at each time slot.

4. **Hysteresis Margin δ:** Represents the minimum required difference in SINR for an alternative beam or RF AP to be considered superior. A smaller hysteresis margin increases the likelihood of completing the monitoring phase and initiating a handover, but also makes the mechanism more susceptible to minor fluctuations or temporary spikes. A larger margin mitigates the impact of such transient changes, but may prevent timely handovers when genuinely needed.

Monitoring phase

While $t_{\text{elapsed}} < t_{\text{dwell}}$, the mechanism performs the following operations at each time slot:

1. **Extract SINR:** Gather the SINR values from all beams and RF APs into an array, as shown in

$$\text{SINR}[i] \leftarrow SINR_i \quad \text{for each } i \in [0, \alpha + \beta), \tag{4.1}$$

   where $SINR_i$ represents the SINR recorded for beam or AP indexed by i, α is the number of NB-OWC beams, and β is the number of RF APs.

2. **Measurement Adjustment:** The SINR values from RF APs are scaled using the network selection coefficient λ, as shown in

$$\gamma = \begin{cases} \text{SINR}, & \text{for NB-OWC beam,} \\ \lambda \times \text{SINR}, & \text{for RF AP,} \end{cases} \tag{4.2}$$

   where γ denotes the adjusted value.

3. **Hysteresis Check:** Identify the set of beams or RF APs whose adjusted SINR exceeds that of the current serving connection by at least the hysteresis margin δ, as shown in

$$\{i \mid \gamma[i] > \gamma_{\text{current\_serving}} + \delta\}, \tag{4.3}$$

If the set is empty (i.e., the current serving connection provides the best SINR), the monitoring phase is terminated, all variables are reset to their initial state, and the procedure is retried in the next time slot.

If the set is non-empty, t_{elapsed} is incremented as shown in

$$t_{\text{elapsed}} \leftarrow t_{\text{elapsed}} + t_{TTT}, \tag{4.4}$$

and the mechanism proceeds to the next time slot.

Figure 4.3 illustrates the operations performed during each step of the monitoring phase.

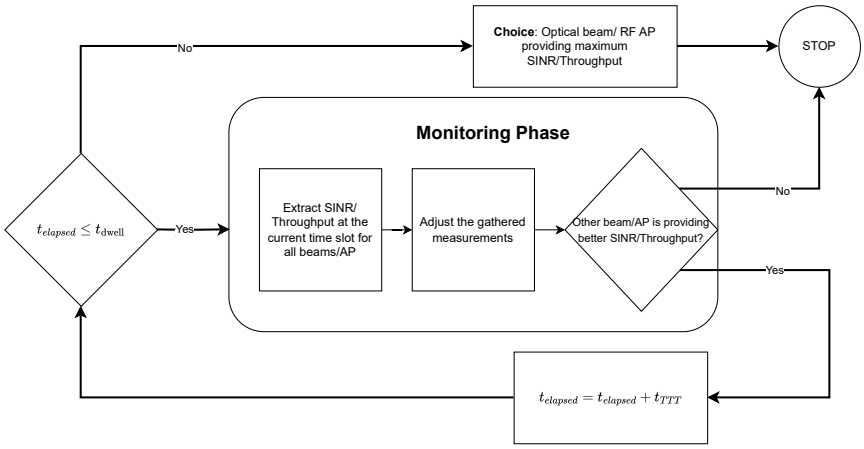

Figure 4.3: **Monitoring phase: Summary of operations**

Decision phase

Once the monitoring phase has been successfully completed, the mechanism selects the beam or RF AP that provides the highest adjusted SINR at the current time slot, as defined in

$$\text{choice} = \arg\max(\gamma[i]), \quad \forall i \in [0, \alpha + \beta). \tag{4.5}$$

4.6.2 Mechanism 2: Reactive Throughput

Mechanism 2 follows the same procedural structure as Mechanism 1, comprising initialisation, monitoring, and decision phases. The key difference lies in the performance metric used: throughput is employed instead of SINR, and no adjustment is made using the network selection coefficient λ.

Monitoring phase

While $t_{\text{elapsed}} < t_{\text{dwell}}$, the mechanism performs the following operations at each time slot:

1. **Extract Throughput:** Gather the achievable throughput from all beams and RF APs into an array, as shown in

$$\mathrm{TP}[i] \leftarrow \mathrm{TP}_i \quad \text{for each } i \in [0, \alpha + \beta), \tag{4.6}$$

   where TP_i represents the throughput recorded for beam or AP indexed by i.

2. **Hysteresis Check:** Identify the set of beams or RF APs whose throughput exceeds that of the current serving connection by at least the hysteresis margin δ, as shown in

$$\{i \mid \mathrm{TP}[i] > \mathrm{TP}_{\text{current\_serving}} + \delta\}, \tag{4.7}$$

   If the set is empty, the monitoring phase is terminated, all variables are reset, and the procedure is retried in the next time slot.

   If the set is non-empty, t_{elapsed} is incremented as shown in (4.4), and the mechanism proceeds to the next time slot.

Decision phase

Once the monitoring phase has been successfully completed, the mechanism selects the beam or RF AP that provides the highest throughput at the current time slot, as defined in

$$\text{choice} = \arg\max(\mathrm{TP}[i]) \quad \forall i \in [0, \alpha + \beta). \tag{4.8}$$

4.7 Predictive mechanisms

Two predictive mechanisms are described in this section. The first, Mechanism 3, uses predicted SINR values to guide handover decisions. The second, Mechanism 4, replaces SINR with predicted throughput as the decision-making metric. Both mechanisms share a common structure comprising initialisation, prediction, and decision phases, and are designed to optimise throughput while maintaining robust connectivity in dynamic environments.

4.7.1 Mechanism 3: Predictive SINR

Initialisation phase

When a handover condition is triggered, the mechanism begins by initialising the following variables:

1. **Current Step k:** For a prediction window of size η, let k denote the individual time slot within the window, where $1 \leq k \leq \eta$, starting at $k = 1$.

2. **Current Time t_k:** Represents the timestamp recorded at the start of the k-th step.

3. **Prediction Step Size t_{TTT}:** Specifies the time interval between two consecutive predictions.

4. **Score:** An array used to track the SINR measurements throughout the execution of the mechanism. It is analysed during the decision phase to determine the optimal beam or AP for handover. Let α and β denote the total number of NB-OWC beams and RF APs in the system, respectively. The score array is of length $(\alpha + \beta)$, where NB-OWC beams are indexed by $i \in [0, \alpha)$ and RF APs by $i \in [\alpha, \alpha + \beta)$. The array is initialised with zero values.

5. **Decay Constant d:** As predictions extend further into the future, they become increasingly dependent on prior estimations, raising the likelihood of deviation from actual user trajectories. To account for this uncertainty, an exponential decay is applied to the score at each time slot. This ensures that predictions further in the future exert less influence on the final decision.

Prediction phase

While $k < \eta$, the mechanism performs the following operations at each prediction slot:

1. **Location Prediction:** The user's location at the $(k+1)$-th slot is predicted using the short-term motion model, given by

$$p(t_k + t_{TTT}) \leftarrow p(t_k) + v(t_k) \times t_{TTT} + \frac{1}{2} a(t_k) \times t_{TTT}^2, \tag{4.9}$$

   where $v(t_k)$ and $a(t_k)$ represent the velocity and acceleration at time t_k.

2. **SINR Estimation:** Based on the predicted location, the mechanism estimates the SINR from each NB-OWC beam and RF AP.

3. **Measurement Adjustment:** The SINR values from RF APs are scaled using the network selection coefficient λ, as shown in

$$\gamma = \begin{cases} \text{SINR}, & \text{for NB-OWC beam}, \\ \lambda \times \text{SINR}, & \text{for RF AP}, \end{cases} \tag{4.10}$$

   where γ denotes the adjusted value.

4. **Score Update:** The score array is updated using the adjusted measurements and the decay factor, as shown in

$$\text{Score}[i] \leftarrow \text{Score}[i] + \gamma_i \times e^{-dk} \quad \text{for each } i \in [0, \alpha + \beta), \tag{4.11}$$

Decision phase

After completing the prediction phase across all time slots, the mechanism selects the beam or RF AP with the highest cumulative score, as defined in

$$\text{choice} = \arg\max(\text{Score}[i]) \quad \forall i \in [0, \alpha + \beta). \tag{4.12}$$

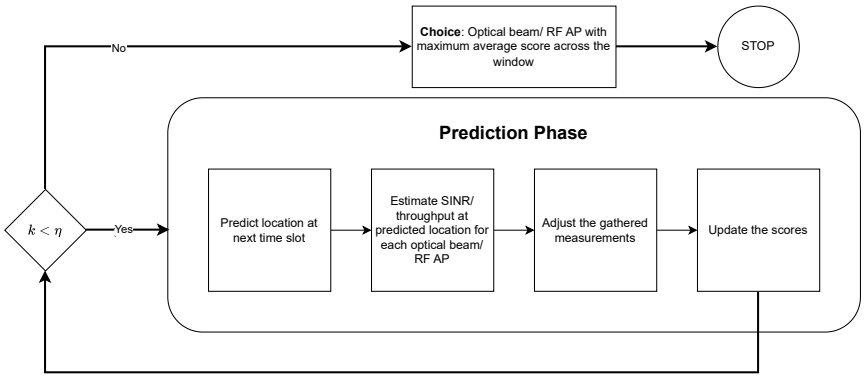

Figure 4.4: **Prediction phase: Summary of operations**

4.7.2 Mechanism 4: Predictive Throughput

Mechanism 4 follows the same structural flow as Mechanism 3, comprising initialisation, prediction, and decision phases. The key distinction lies in the performance metric used: throughput is employed instead of SINR, and no adjustment is made using the network selection coefficient λ.

Prediction phase

At each time slot within the prediction window, the mechanism estimates the throughput from each NB-OWC beam and RF AP based on the predicted user location. The score array is updated using the estimated throughput values and the exponential decay factor, as shown in

$$\text{Score}[i] \leftarrow \text{Score}[i] + \text{Throughput}_i \times e^{-dk} \quad \text{for each } i \in [0, \alpha + \beta), \tag{4.13}$$

Decision phase

The final handover decision is made by selecting the beam or RF AP with the highest cumulative score across the prediction window, using the same decision logic as in Mechanism 3:

$$\text{choice} = \arg\max(\text{Score}[i]) \quad \forall i \in [0, \alpha + \beta). \tag{4.14}$$

This chapter introduced four handover mechanisms for mobility management in narrow beam systems, grouped into reactive and predictive mechanisms. Reactive mechanisms operate reactively using real-time measurements, with Mechanism 1 based on SINR and Mechanism 2 on throughput. Predictive mechanisms, Mechanisms 3 and 4, incorporate user trajectory estimation to evaluate future connectivity, using predicted SINR and throughput respectively. All mechanisms aim to maximise throughput while maintaining stable connectivity, with design choices such as dwell time, hysteresis, prediction windows, and decay constants tailored to balance responsiveness and reliability. These mechanisms form the basis for the performance evaluation presented in the next chapter.

Chapter 5

Evaluation setup and results

This chapter presents the simulation scenario and evaluates the performance of the three proposed handover mechanisms introduced in Chapter 4 in comparison to the baseline from literature [76]. The evaluation is conducted under a controlled single-user mobility scenario based on the RWP model as elaborated on in Section 3.3.1. The aim is to analyse and compare the mechanisms with respect to throughput and handover behaviour under indoor mobility conditions.

The chapter begins by outlining the simulation setup, detailing the network configuration, and performance metrics. Subsequently, results from an initial comparative run are presented, offering a high-level performance comparison across mechanisms. This is followed by a per-run analysis, where we examine the detailed behaviour of each mechanism over time during a representative user trajectory, in order to understand how each mechanism responds in mobility conditions. The impact of key parameters on mechanism performance is then explored individually: the hysteresis margin, the network selection coefficient λ, and the prediction window size η. Finally, the chapter concludes with a performance analysis after parameter optimisation, highlighting the trade-offs and comparative strengths of predictive versus baseline approaches.

5.1 Simulation scenario

This section outlines the simulation scenario used to evaluate the performance of the four handover mechanisms introduced in Chapter 4. The evaluation is conducted in an indoor, single-room environment representative of common user spaces such as offices or meeting rooms. The focus is on mobility-driven handovers, where transitions between access points or beams are predominantly triggered by user movement.

The UE moves according to the RWP mobility model, which introduces realistic, non-uniform movement patterns by combining random pauses with directed motion. To assess robustness under varying mobility conditions, each mechanism is evaluated across multiple user speeds. The scenario is designed to observe how the different mechanisms adapt to these varying speeds.

Table 5.1: **Simulation parameters used in the evaluation**

Parameter	Description	Value
N_{sim}	Number of simulation instances run for evaluation	100
N_{steps}	Number of time steps per simulation instance	20,000
τ_{step}	Duration of each time step	5 ms
T_{sim}	Total time per simulation instance	100 s
X_{dim}	Width of the simulation space	5 m
Y_{dim}	Height of the simulation space	5 m
User speeds	User speeds being evaluated	[0.1, 0.5, 1, 2, 3, 4, 5, 6, 7, 8, 9, 10] m/s

The following subsections detail the simulation parameters, network configuration, and performance metrics used in the evaluation.

5.1.1 Simulation parameters

The simulation environment was configured to assess handover mechanisms under indoor mobility conditions. Table 5.1 lists the parameters used.

Each simulation instance runs for a total duration of $T_{\text{sim}} = 100$ s, divided into $N_{\text{steps}} = 20{,}000$ time steps, with each step lasting $\tau_{\text{step}} = 5$ ms. A total of $N_{\text{sim}} = 100$ independent instances were executed to ensure statistical robustness. The simulation space is defined as a 5 m$\times$5 m area, representing a typical indoor environment.

Simulating over a 100-second duration offers a key advantage: it reduces variability in performance metrics, particularly at lower user speeds. For speeds below 1m/s, shorter simulation times can result in too few handover events, making the performance heavily dependent on the user's initial position rather than the true efficacy of the handover mechanism. A longer simulation ensures that, even at 0.1m/s, the user traverses 10m, sufficient to engage with multiple access points or beams and trigger meaningful handover decisions. The choice of 100s thus provides an optimal compromise between capturing representative mobility dynamics and maintaining reasonable computational cost for large-scale simulation runs.

These settings provide sufficient temporal and spatial resolution to capture mobility dynamics and handover events with accuracy.

5.1.2 Network parameters

The simulation scenario includes a hybrid indoor network comprising a Wi-Fi and a NB-OWC system, each represented by a single AP located centrally within the simulation space. The UE connects to one network at a time, with VHO events triggered based on performance criteria.

The configuration of the NB-OWC network is summarised in Table 5.2. These parameters are adopted from [41] and [67], and reflect a double-tier AP design with 225 VCSELs arranged in a 3×3 grid of 5×5 arrays. The system operates

Table 5.2: **NB-OWC network parameters**

Parameter	**Description**	**Value**
h_{DL}	Vertical separation	3 m
ω_0	Beam waist radius	4 μm
λ	VCSEL wavelength	975 nm
P_t	Transmit optical power per VCSEL	10 mW
RIN	RIN PSD	-155 dB/Hz
n_{lens}	Lens refractive index	1.55
R_{PD}	PD responsivity	0.7 A/W
N_{PD}	Number of PDs in the matrix	25
A_{PD}	Area of the PD matrix	2 cm^2
R_L	Load resistance	50 Ω
F_n	TIA noise figure	5 dB
B	System bandwidth	2 GHz
BER	Pre-FEC BER	10^{-3}
ζ	Utilisation factor	0.93

Table 5.3: **Wi-Fi network parameters**

Parameter	**Description**	**Value**
$P_{\text{Wi-Fi}}$	Transmitted power for Wi-Fi AP	20 dBm
$B_{\text{Wi-Fi}}$	System bandwidth of Wi-Fi AP	20 MHz
$N_{\text{Wi-Fi}}$	PSD of noise in Wi-Fi	-174 dBm/Hz
$\zeta_{\text{Wi-Fi}}$	Utilisation factor for Wi-Fi	0.7

at a wavelength of 975 nm, with a bandwidth of 2 GHz and a responsivity of 0.7 A/W.

Table 5.3 outlines the Wi-Fi network parameters, which are based on the configuration proposed in [77]. The AP provides isotropic coverage with a transmit power of 20 dBm and a bandwidth of 20 MHz.

These parameters are used to compute SINR and throughput as modelled in Chapter 3.

5.1.3 Performance metrics

We evaluate the performance of the proposed mechanisms using the following three metrics:

- **Average user experienced throughput (Gb/s):** The mean throughput experienced by the user, computed over all simulation instances and time steps. This serves as a primary indicator of the overall user performance delivered by each mechanism.
- **10^{th} percentile user throughput (Gb/s):** The average of the 10^{th} percentile user throughput values recorded across all simulation runs and time steps. This metric captures the lower-bound user experience, helping to identify scenarios where a mechanism may fail to initiate timely handovers, potentially leading to degraded connectivity or temporary disconnections despite high average user throughput.

Table 5.4: **Default parameters for initial comparative run**

Parameter	Description	Default value
λ	Wi-Fi preference coefficient	1
η	Prediction window size	5
δ_{SINR}	Hysteresis margin for SINR-based methods	1 dB
t_{dwell}	Dwell time for reactive methods	25 ms
t_{wait}	Wait time for predictive methods	25 ms

- **Average handover rate (s^{-1}):** The average number of handovers executed per second by a given mechanism. This metric reflects the balance between responsiveness and stability, and helps assess whether frequent handovers introduce overheads that adversely affect user throughput.

5.2 Results and observations

5.2.1 Initial comparative run

This subsection presents a baseline performance comparison of the three proposed handover mechanisms against the baseline under default parameter settings. Table 5.4 summarises the parameters used in this run.

The default value of $\lambda = 1$ is chosen to neutralise its effect, as per the formulation in Equation (4.2), where $\lambda = 1$ results in equal weighting between RF and NB-OWC networks. The hysteresis margin δ_{SINR} is set to 1 dB to ensure handovers are triggered under realistic conditions while avoiding excessive ping-ponging. The prediction window size $\eta = 5$ is selected to allow meaningful evaluation of predictive mechanisms over multiple steps, while limiting the impact of trajectory deviation at higher speeds. The dwell time for reactive mechanisms and the wait time t_{wait} for predictive mechanisms are both set to 25 ms. Here, t_{wait} defines the minimum interval between two consecutive handovers in predictive mechanisms, helping to reduce unnecessary computation and excessive handover frequency. This alignment ensures that both reactive and predictive handover mechanisms operate under comparable overhead assumptions.

Average user Throughput: Figure 5.1a illustrates the average user throughput achieved by each mechanism across varying user speeds. Predictive throughput mechanism consistently delivers the highest performance, particularly in the mid-to-high speed range, owing to its preference for the NB-OWC network, which provides superior capacity. This preference arises from its throughput-based scoring, which inherently favours NB-OWC systems. A more detailed discussion of this behaviour is provided in Section 5.2.4.

Both reactive mechanisms exhibit a sharp decline in user throughput with the increase of speed up to 5 m/s, after which performance stabilises. This is attributed to the fact that the mechanisms are more likely to switch to the Wi-Fi network as the speed increases, as corroborated by the plateau in handover rate beyond 5 m/s (Figure 5.1c). The predictive SINR mechanism also shows

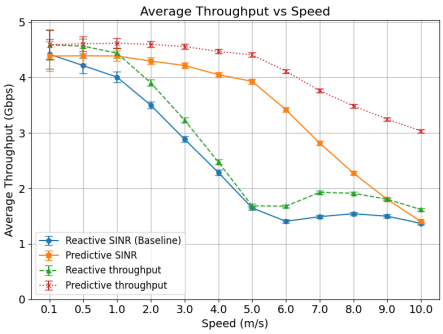

(a) **Comparison of average user throughput between the 4 mechanisms for the initial simulation setup**

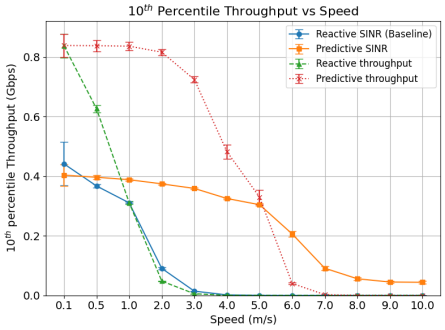

(b) **Comparison of 10th percentile user throughput between the 4 mechanisms for the initial simulation setup**

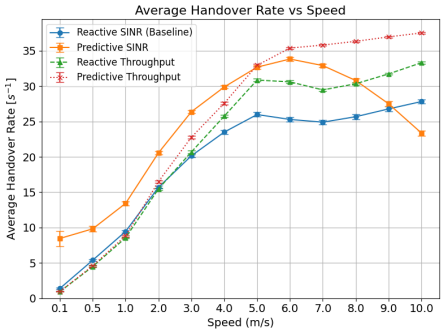

(c) **Comparison of average handover rate between the 4 mechanisms for the initial simulation setup**

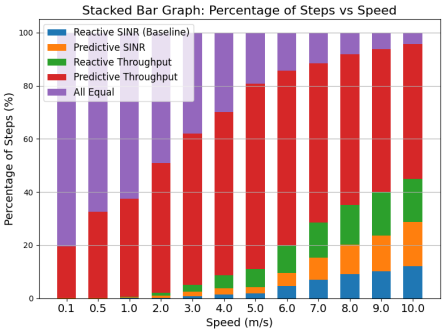

(d) **(%) dominance comparison between the 4 mechanisms for the initial simulation setup**

Figure 5.1: **Results from initial comparative run**

a marked drop in user throughput beyond 5 m/s, suggesting that the default η value becomes insufficient at maintaining high average user throughput at higher speeds.

Interestingly, the predictive throughput mechanism does not suffer from this limitation. Its user throughput remains high and handover rate continues to increase with speed. The underlying reasons for this divergence are explored further in Section 5.2.4.

10th Percentile user Throughput. Figure 5.1b presents the 10th percentile user throughput, capturing the lower-bound user experience. All mechanisms show a sharp decline in performance with increasing speed, with reactive methods reaching near-zero values earlier than predictive ones. Predictive SINR mechanism stabilises around the speed of 8 m/s, never reaching zero, due to its tendency to switch to Wi-Fi and maintain connectivity, albeit at reduced performance.

Reactive mechanisms suffer from disconnections at higher speeds. This is because their final handover decision is based solely on the current time step following the monitoring phase, without considering future performance. At high speeds, the user may traverse an entire NB-OWC beam in a single time step, leading to transient optimality followed by disconnection.

Predictive throughput mechanism, by contrast, heavily favours NB-OWC due to the scale difference in user throughput (Gb/s vs Mb/s). It maintains the user in the optical network as long as possible, resulting in higher average user throughput and increasing handover rate. However, its reluctance to perform vertical handovers eventually leads to disconnections beyond the speed of 7 m/s, as even predictions fail to compensate for rapid mobility.

Average Handover Rate. Figure 5.1c shows the average number of handovers per second for each mechanism. As expected, handover rates increase with the increase of user speed across all mechanisms. However, the nature of this increase varies and is closely linked to user throughput performance.

For both reactive mechanisms, the handover rate rises sharply in the speed range up to 5 m/s and then plateaus. This behaviour aligns with the observed drop and stabilisation in user throughput (Figure 5.1a), as the mechanisms tend to switch to the Wi-Fi network. Since reactive methods only consider current performance, they switch to Wi-Fi when it becomes momentarily superior.

Predictive SINR mechanism, in contrast, exhibits a decline in handover rate at speeds beyond 5 m/s. This is due to its anticipatory nature: the mechanism predicts that Wi-Fi will offer more stable performance across the prediction window and thus proactively switches and remains connected. This strategic shift reduces the need for frequent handovers but also leads to a drop in user throughput, as NB-OWC is underutilised.

Predictive throughput mechanism continues to increase its handover rate with the increase of speed. This mechanism strongly favours NB-OWC due to its higher user throughput potential and attempts to maintain connectivity with it as long as possible. As a result, it performs frequent handovers to adapt to the user's movement across NB-OWC beams. While this leads to higher user throughput, it also increases the risk of disconnections at very high speeds, as discussed in the 10th percentile analysis.

Table 5.5: **Hysteresis margins observed**

Parameter	Values simulated
δ_{SINR}	[0.01, 0.5, 1.0, 3.0, 5.0, 7.0, 10.0] dB

Dominance Comparison. Figure 5.1d presents a stacked bar chart showing the percentage of simulation steps where each mechanism was providing the best user throughput. At lower speeds, all mechanisms perform similarly, with a high proportion of steps marked as "All Equal". As speed increases, predictive throughput mechanism begins to dominate, peaking around 6 m/s. Beyond this point, its dominance plateaus, and other mechanisms begin to gain ground. This trend aligns with the observations from the 10th percentile user throughput graph and reflects the growing limitations of predictive throughput mechanism at very high speeds.

The baseline comparison shows that predictive throughput mechanism achieves the highest average performance, particularly at moderate speeds, but its strong preference for optical links results in disconnections under rapid mobility. Reactive mechanisms suffer sharp performance degradation and frequent disconnections at even low to moderate speeds. Predictive SINR mechanism offers greater stability by proactively switching to Wi-Fi, though at the cost of reduced user throughput. These results establish the performance trade-offs of each approach and provide a reference point for evaluating parameter variations in later analyses.

5.2.2 Effect of hysteresis margin

This subsection evaluates the impact of varying the hysteresis margin δ_{SINR} on the performance of SINR-based handover mechanisms. Table 5.5 lists the range of hysteresis values considered in the simulation. The aim is to understand how this parameter influences user throughput, handover rate, and overall stability[1].

Across both reactive and predictive mechanisms, a consistent trend is observed: as the hysteresis margin increases, average user throughput (Figures 5.2a and 5.2b), 10th percentile user throughput (Figures 5.2c and 5.2d), and handover rate (Figures 5.2e and 5.2f) all decrease. This behaviour is expected, as a higher hysteresis margin raises the threshold required to trigger a handover. Consequently, handovers are either delayed or entirely suppressed, leading to reduced responsiveness and lower user throughput. The reduction in handover rate is a direct result of fewer transitions being executed under stricter conditions.

A key distinction between the two mechanisms lies in the degree to which hysteresis margin affects their performance. The reactive mechanism is significantly more sensitive to changes in δ_{SINR} than the predictive mechanism. This difference stems from their operational structure: in reactive methods, the

[1] A similar hysteresis analysis is not performed for throughput-based handovers, which use a fixed margin of 1 Mb/s to allow the Wi-Fi network any chance of providing higher user throughput than NB-OWC, which delivers user throughput on the order of Gb/s. Due to this large disparity, any reasonable hysteresis margin already saturates performance, and user throughput at 0 Mb/s and 1 Mb/s margins is effectively identical. Therefore, varying the margin for throughput-based mechanisms is not considered.

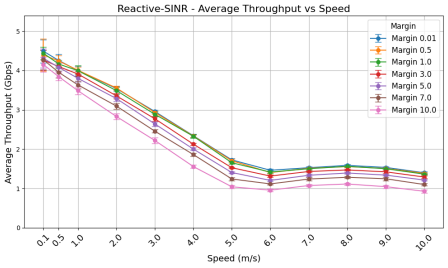

(a) **Reactive SINR: Average user throughput across different hysteresis margin**

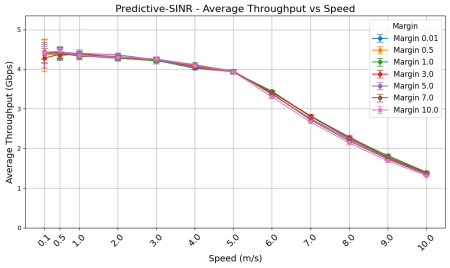

(b) **Predictive SINR: Average user throughput across different hysteresis margin**

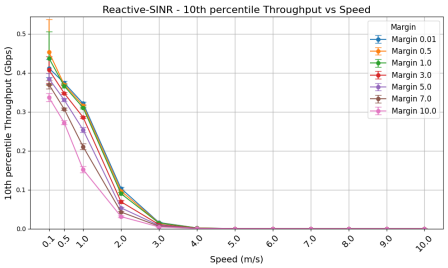

(c) **Reactive SINR: 10th percentile user throughput across different hysteresis margin**

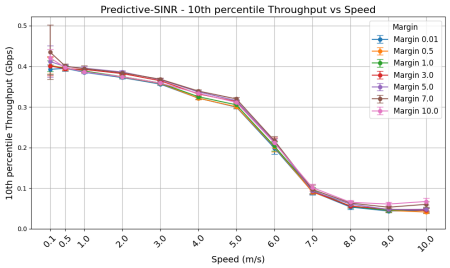

(d) **Predictive SINR: 10th percentile user throughput across different hysteresis margin**

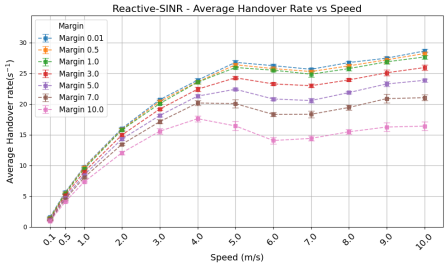

(e) **Reactive SINR: Average handover rate across different hysteresis margin**

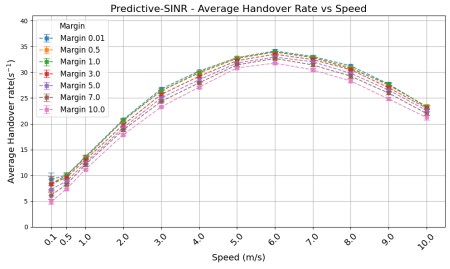

(f) **Predictive SINR: Average handover rate across different hysteresis margin**

Figure 5.2: **Evaluating the effect of hysteresis margin on performance metrics**

Table 5.6: **Lambda parameter values observed**

Parameter	Values simulated
λ	0.1, 0.5, 1.0, 3.0, 5.0, 7.0, 10.0

hysteresis margin is applied during every time slot of the monitoring phase, requiring alternative beams or access points to consistently outperform the current connection by the margin. In contrast, predictive methods apply the hysteresis margin only once during the initialisation phase, as a preliminary check before executing the prediction and decision phases. As such, the margin plays a more dominant role in reactive decision-making.

Notably, a hysteresis margin of 1 dB appears to be a saturation point. Below this threshold, no appreciable improvements are observed in user throughput or handover rate. The performance metrics for $\delta_{\text{SINR}} = 0.01$, 0.5, and 1.0 dB are nearly identical, indicating diminishing returns from further reducing the margin.

While lower hysteresis margins yield higher user throughput and improved 10th percentile performance, they also result in increased handover rates. However, as demonstrated in the initial comparative run (Section 5.1), higher handover rates are positively correlated with user throughput at the speeds considered. This is primarily due to the user remaining connected to the NB-OWC network for longer durations, which offers superior data rates. In this regime, handover rate does not yet constitute a performance bottleneck. Therefore, a hysteresis margin of 1 dB is deemed optimal, offering the best balance across all evaluated metrics.

5.2.3 Effect of λ parameter

This subsection investigates the influence of the network selection coefficient λ on the performance of SINR-based handover mechanisms. Table 5.6 lists the values evaluated. The parameter λ modulates the system's preference for RF connectivity, particularly under high mobility conditions. Originally proposed for hybrid Li-Fi/Wi-Fi networks, its role must be reinterpreted for NB-OWC systems due to the significant disparity in achievable user throughput. The aim here is to understand how varying λ affects user throughput and handover rate across different speeds.

In terms of average user throughput (Figures 5.3a and 5.3b), the effect of λ is direct and intuitive: lower values result in higher user throughput. This is because lower λ values reduce the system's bias towards the Wi-Fi network, favouring NB-OWC instead, which offers significantly higher data rates.

The 10th percentile user throughput (Figures 5.3c and 5.3d) exhibits a more nuanced behaviour. At lower speeds, the trend mirrors that of average user throughput, lower λ yields better performance. However, beyond a certain speed threshold, this relationship reverses. For the reactive mechanism, the switch occurs around 1 m/s, while for the predictive mechanism, it occurs closer to 5 m/s. This indicates that at higher speeds, maintaining connectivity becomes more challenging within the NB-OWC domain alone. The predictive mechanism, with its ability to anticipate future conditions, is more resilient to mobility and can sustain NB-OWC connectivity longer than the reactive mechanism.

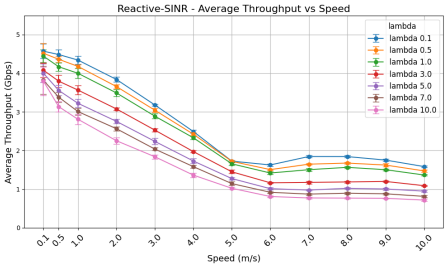

(a) **Reactive SINR: Average user throughput across different lambda values**

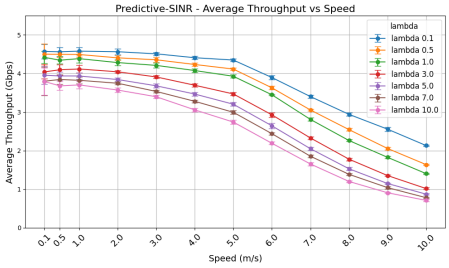

(b) **Predictive SINR: Average user throughput across different lambda values**

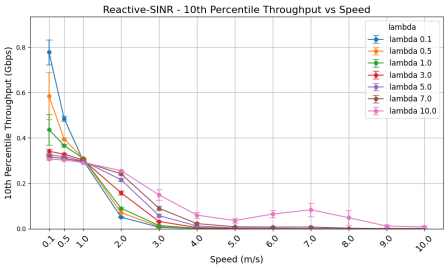

(c) **Reactive SINR: 10th percentile user throughput across different lambda values**

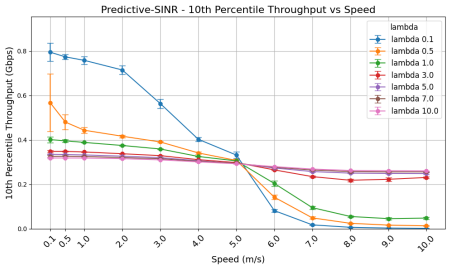

(d) **Predictive SINR: 10th percentile user throughput across different lambda values**

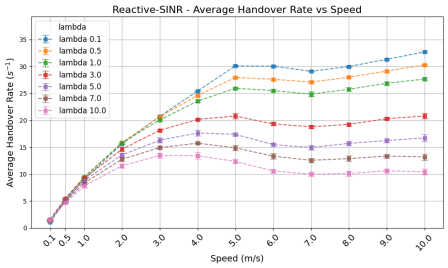

(e) **Reactive SINR: Average handover rate across different lambda values**

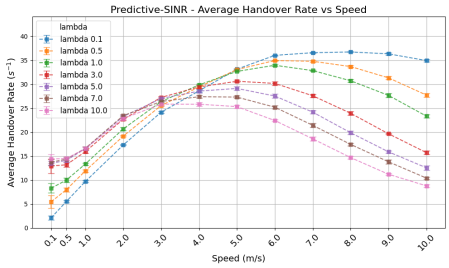

(f) **Predictive SINR: Average handover rate across different lambda values**

Figure 5.3: **Evaluating the effect of lambda parameter on performance metrics**

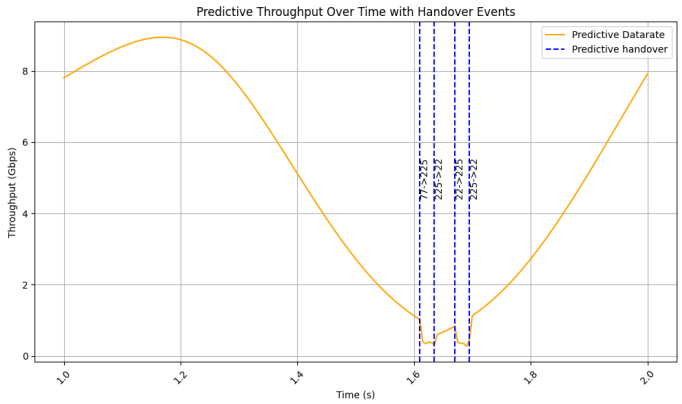

Figure 5.4: **Handovers initiated by the predictive mechanism over a 1 second time period. Here 225 is the index of the Wi-Fi AP.**

The average handover rate (Figures 5.3e and 5.3f) follows a similar trend to the 10th percentile user throughput, though the effect is more pronounced in the predictive mechanism. At lower speeds, lower λ values reduce the likelihood of switching to Wi-Fi, keeping the user within the NB-OWC system and thereby reducing handovers. At 0.1 m/s, the predictive mechanism performs unnecessary handovers by switching to the Wi-Fi network despite the NB-OWC system offering better user throughput overall (higher SINR need not mean higher user throughput). This behaviour is illustrated in Figure 5.4, where the mechanism temporarily favours Wi-Fi due to its higher SINR across the prediction window, only to switch back to NB-OWC shortly after, increasing the handover count. This behavior is avoided with lower lambda values. However, beyond the threshold speed of 5m/s, maintaining NB-OWC connectivity requires frequent handovers due to the user's traversal across multiple beam coverage areas. Thus, lower λ values lead to increased handover rates at higher speeds.

These observations highlight a trade-off in configuring λ. Below 5m/s, lower values of lambda improve user throughput and reduce handovers. Beyond 5m/s, however, lower values of lambda may compromise connectivity and increase handover overhead. If the system prioritises user throughput, a lower λ is preferable. If connectivity is paramount, a higher λ is more suitable.

For the purposes of this thesis we set the lambda values accordingly: for the reactive mechanism, λ is set to 0.1 across all speeds, as higher values offer negligible improvement in 10th percentile user throughput but significantly reduce average user throughput. For the predictive mechanism, λ is set to 0.1 below the threshold of 5 m/s and 1.0 beyond it, balancing user throughput and connectivity.

5.2.4 Effect of η parameter

This subsection evaluates the impact of the prediction window size η on the performance of the predictive SINR mechanism and predictive throughput mechanisms. Table 5.7 lists the values considered. The parameter η determines how far into the future the mechanism forecasts user location and correspond-

Table 5.7: **Eta parameter values observed**

Parameter	Values simulated
η	1.0, 2.0, 3.0, 4.0, 5.0, 6.0, 7.0, 8.0, 9.0, 10.0

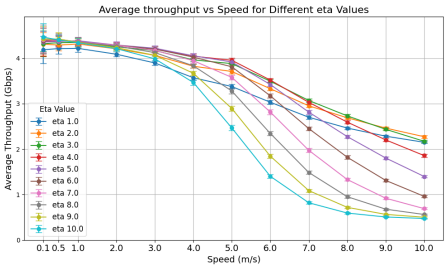

(a) **Predictive SINR: Average user throughput across different eta values**

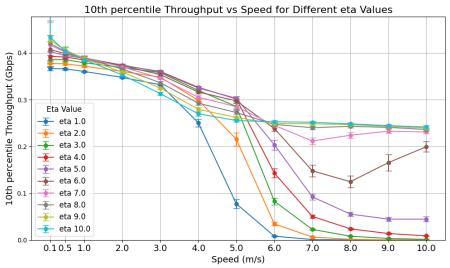

(b) **Predictive SINR: 10th percentile user throughput across different eta values**

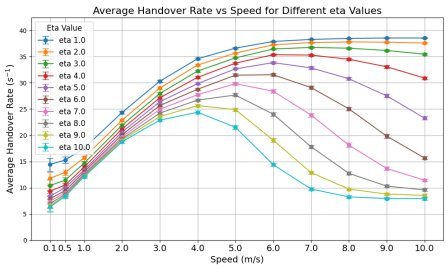

(c) **Predictive SINR: Average handover rate across different eta values**

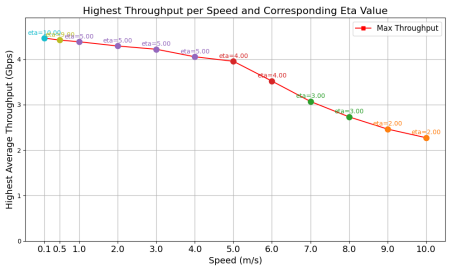

(d) **Predictive SINR: Eta value selection for maximum average user throughput**

Figure 5.5: **Evaluating the effect of eta parameter on performance metrics for the predictive SINR mechanism**

ing performance metrics before making a handover decision. Its value directly influences the mechanism's ability to anticipate mobility-induced changes and maintain optimal connectivity. The aim is to understand how varying η affects user throughput, handover rate, and resilience to user movement across different speeds.

Predictive SINR Mechanism. For the predictive SINR mechanism, the effect of η on average user throughput (Figure 5.5a) is pronounced. As η increases, the curvature of the user throughput curve increases, especially at higher speeds. An η value of 1 is functionally equivalent to a reactive method without a monitoring phase, making decisions based solely on current conditions. A clear trend emerges: higher η values perform better at lower speeds, while lower η values are preferable at higher speeds.

At low speeds, user movement per time step is minimal and more predictable, aligning well with the linear motion assumption of the prediction model. Additionally, a larger prediction window allows the user to fully transition into the

coverage area of the next NB-OWC beam, avoiding unnecessary handovers to Wi-Fi. At higher speeds, however, the user spends less time within any single optical beam's coverage area. As a result, no NB-OWC beam accumulates sufficient SINR across the prediction window, while the Wi-Fi network provides consistent SINR. This leads to a bias towards Wi-Fi, especially with large η values such as $\eta = 10$, where the user may remain permanently in the Wi-Fi network.

The 10th percentile user throughput (Figure 5.5b) exhibits an inverse trend. At higher speeds, larger η values improve lower-bound performance by favouring Wi-Fi, which ensures connectivity even if user throughput is lower. At lower speeds, smaller η values result in more frequent transitions and potential disconnections, reducing 10th percentile performance.

The average handover rate (Figure 5.5c) decreases with increasing η. Smaller η values lead to more frequent handovers, especially at higher speeds, while larger η values reduce transitions by favouring stable Wi-Fi connectivity. At low speeds, larger η values also help avoid ping-pong handovers between NB-OWC and Wi-Fi.

Figure 5.5d maps the optimal η value for maximum average user throughput across speeds. The trend confirms the earlier observations: optimal η decreases as speed increases. At low speeds, larger η values provide stability and prevent unnecessary transitions; at high speeds, smaller η values allow continued utilisation of NB-OWC.

Overall, a trade-off emerges beyond 5 m/s. Lower η values maximise user throughput but may compromise reliability. Higher η values ensure connectivity via Wi-Fi but reduce user throughput. For this thesis, we adopt the η values indicated in Figure 5.5d, prioritising average user throughput, as the gains outweigh the minor losses in 10th percentile performance.

Predictive throughput Mechanism. For the predictive throughput mechanism, the impact of η on average user throughput (Figure 5.6a) is less pronounced. All η values perform similarly, with $\eta = 5$ yielding the best results and $\eta = 1$ performing the worst. This difference arises from the scoring metric: user throughput rather than SINR. While SINR values for NB-OWC and Wi-Fi are comparable, user throughput differs significantly (Gb/s vs Mb/s), strongly favouring NB-OWC in the scoring process. Consequently, the mechanism tends to remain within the NB-OWC domain regardless of η, except for $\eta = 1$, which behaves like a reactive method and may occasionally favour Wi-Fi due to transient conditions.

The optimality of $\eta = 5$ is attributed to its alignment with the dwell time $t_{\text{wait}} = 25$ ms, ensuring synchronisation between prediction and decision intervals.

For 10th percentile user throughput (Figure 5.6b), $\eta = 5$ again performs best. No clear correlation is observed between η and performance, aside from proximity to $\eta = 5$, values such as $\eta = 4$ and $\eta = 6$ perform better than extremes like $\eta = 1$ or $\eta = 10$.

The handover rate (Figure 5.6c) follows a clear trend: lower η values result in more handovers. This mirrors the behaviour observed in the SINR-based mechanism. Smaller η values lead to less anticipatory decisions, increasing the likelihood of additional handovers shortly after the current one. Larger η values

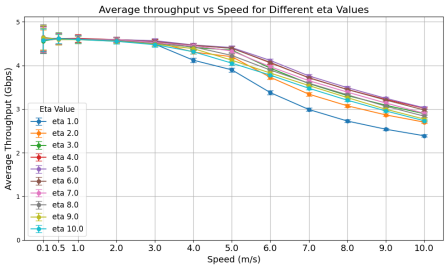

(a) **Predictive throughput: Average user throughput across different eta values**

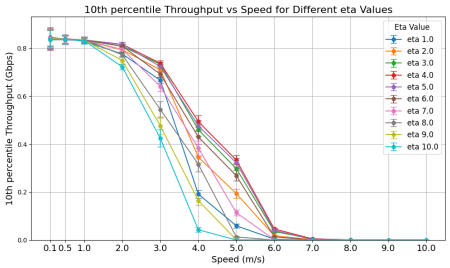

(b) **Predictive throughput: 10th percentile user throughput across different eta values**

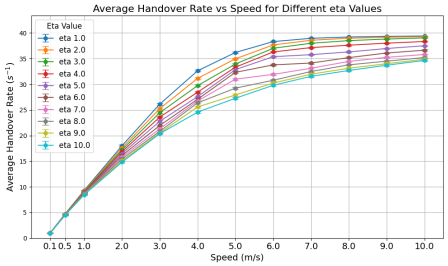

(c) **Predictive throughput: Average handover rate across different eta values**

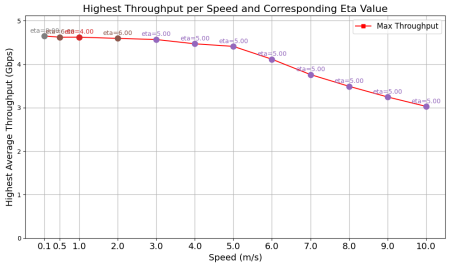

(d) **Predictive throughput: Eta value selection for maximum average user throughput**

Figure 5.6: **Evaluating the effect of eta parameter on performance metrics for the predictive throughput mechanism**

Table 5.8: **Final parameter allocation for each speed value**

m/s	**0.1**	**0.5**	**1.0**	**2.0**	**3.0**	**4.0**	**5.0**	**6.0**	**7.0**	**8.0**	**9.0**	**10.0**
$\lambda_{\text{reactive}}$	0.1	0.1	0.1	0.1	0.1	0.1	0.1	0.1	0.1	0.1	0.1	0.1
$\lambda_{\text{predictive}}$	0.1	0.1	0.1	0.1	0.1	0.1	1.0	1.0	1.0	1.0	1.0	1.0
η_{SINR}	10	9	5	5	5	5	4	4	3	3	2	2
$\eta_{\text{Throughput}}$	5	5	5	5	5	5	5	5	5	5	5	5

provide more foresight, reducing the need for frequent transitions.

Figure 5.6d confirms that $\eta = 5$ is optimal across most speeds. Variations observed with other η values are minor and tend to average out across multiple simulation seeds.

Accordingly, for this thesis, we adopt $\eta = 5$ across all speeds for the predictive throughput mechanism. This choice offers the best balance between average and 10th percentile user throughput.

5.2.5 Performance analysis post optimisations

This subsection presents the performance of all four handover mechanisms after applying parameter optimisation across different user speeds. The tuned values for λ and η are summarised in Table 5.8. The goal is to evaluate how well each mechanism performs when tuned for its respective strengths, and to highlight the trade-offs between user throughput and handover rate. The results provide a comprehensive comparison under realistic mobility conditions, offering insight into the relative advantages of predictive versus reactive mechanisms.

Average user Throughput. Figure 5.7a shows the average user throughput across all mechanisms post optimisation. With $\lambda = 0.1$, the difference between the reactive SINR and reactive throughput mechanisms becomes minimal. While the throughput-based method retains a slight edge due to its reduced tendency to switch to Wi-Fi, the improvement is marginal. Both reactive mechanisms continue to underperform compared to their predictive counterparts.

At a representative speed of 5 m/s, the predictive throughput mechanism achieves a 157.48% improvement in average user throughput over the reactive SINR baseline, while predictive SINR mechanism yields a 131.27% improvement. In contrast, the reactive throughput mechanism offers only a 4.70% gain over the reactive SINR method. These results highlight the substantial advantage of predictive mechanisms in maintaining high data rates under moderate mobility, especially when tuned for user throughput.

10th Percentile user Throughput. Figure 5.7b presents the 10th percentile user throughput. Even after optimisation, the reactive mechanisms exhibit a steep decline, indicating their inability to maintain reliable connectivity at moderate to high speeds. The predictive mechanisms perform significantly better. However, optimising predictive SINR mechanism for average user throughput results in reduced 10th percentile performance, which drops to zero at 8 m/s. predictive throughput mechanism maintains superior performance up to 5 m/s,

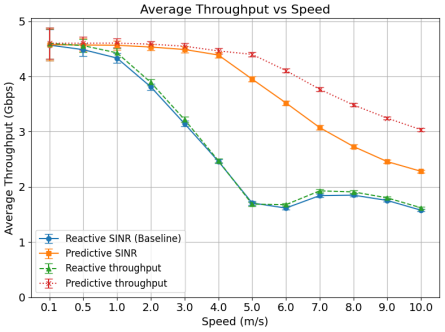

(a) **Comparison of average user throughput between the 4 mechanisms post optimisation**

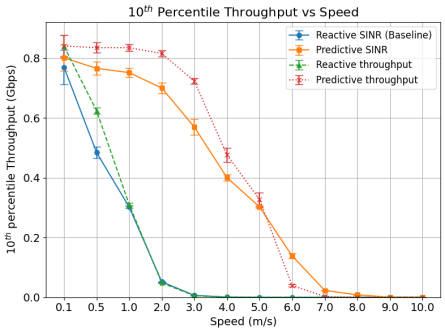

(b) **Comparison of 10th percentile user throughput between the 4 mechanisms post optimisation**

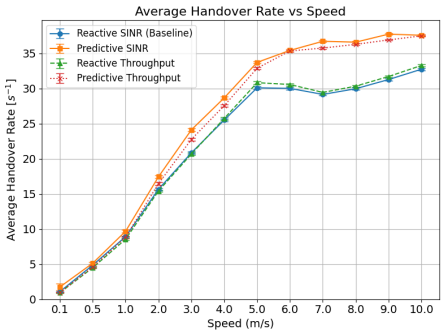

(c) **Comparison of average handover rate between the 4 mechanisms post optimisation**

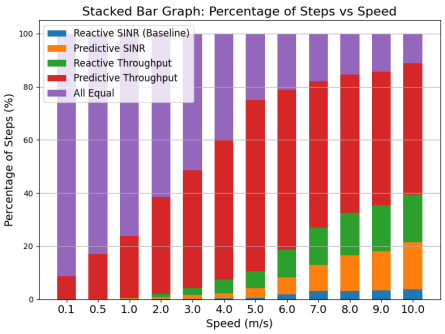

(d) **(%) dominance comparison between the 4 mechanism post optimisation**

Figure 5.7: **Results from comparative runs post optimisation**

but its reluctance to switch to Wi-Fi begins to impact its lower-bound performance at higher speeds, despite retaining higher average user throughput.

Average Handover Rate. Figure 5.7c shows the average handover rate. Similar to the initial run, reactive mechanisms plateau in handover rate beyond moderate speeds. Predictive mechanisms do not exhibit as abrupt a plateau. Optimisation leads to comparable handover rates across all mechanisms at lower speeds, with predictive methods showing only slightly higher rates overall.

Cumulative Dominance Matrix. Figure 5.7d illustrates the percentage of simulation steps where each mechanism was dominant. At very low speeds, performance convergence across mechanisms is reflected in the increased proportion of "All Equal" steps. predictive throughput mechanism continues to dominate until around 5 m/s, after which its percentage share plateaus. predictive SINR mechanism gains a larger portion compared to the initial run, while the reactive baseline mechanism loses ground and plateaus earlier.

These results confirm that predictive mechanisms, when properly tuned, offer superior performance across most metrics. Reactive methods remain limited in their ability to adapt to mobility, even under optimised conditions. The trade-offs between user throughput and reliability are most evident in the predictive SINR mechanism, where tuning for one metric can adversely affect another.

Chapter 6

Conclusions

This thesis investigated mobility-aware handover mechanisms for hybrid RF and NB-OWC networks. Motivated by the limitations of reactive SINR-based handover mechanisms in ultra-dense NB-OWC deployments, the study proposed three distinct handover algorithms, one reactive (throughput-based) and two predictive (SINR-based, throughput-based), designed to reach different trade-offs between user throughput and connectivity performance under varying mobility conditions. These were evaluated against a baseline reactive SINR-based mechanism adapted from existing literature, enabling a comparative analysis of performance improvements and trade-offs.

The system was modelled to reflect realistic indoor environments, incorporating detailed channel and user mobility models. A simulation framework was developed to evaluate the mechanisms across a range of user speeds, using performance metrics including average user throughput, 10^{th} percentile user throughput, and handover rate. Key parameters such as hysteresis margin, network selection coefficient λ, and prediction window size η were analysed to understand their influence on performance.

6.1 Summary of key findings

The evaluation presented in Chapter 5 yielded several important insights:

- **Predictive mechanisms outperform reactive ones:** Both predictive methods demonstrated superior performance in average and 10^{th} percentile user throughput. At a representative speed of 5 m/s, the predictive throughput mechanism achieved a **157% improvement** in average user throughput over the reactive SINR baseline, while predictive SINR yielded a **131% improvement**. In contrast, the reactive throughput mechanism offered only a **4.7% gain**. These results validate the efficacy of prediction-based handover mechanisms, which anticipate user mobility rather than relying solely on reactive user performance monitoring.

- **Trade-off between average and 10^{th} percentile user throughput:** Beyond the speed of 5 m/s, an antagonistic relationship emerges between the two metrics. Handover mechanisms optimised for average user

throughput tend to degrade 10^{th} percentile performance, while those preserving lower-bound user throughput often sacrifice average user throughput. Network designers may therefore prioritise one metric over the other based on application requirements.

- **Correlation between handover rate and average user throughput:** Maintaining high average user throughput necessitates keeping the user within the NB-OWC system. At higher speeds, this requires frequent handovers to adjacent beams, resulting in a positive correlation between user throughput and handover rate.

- **Tuned hysteresis margin:** A hysteresis margin of **1 dB** was identified as optimal for SINR-based mechanisms. It also represents a saturation point, as further reductions (e.g., 0.5 dB or 0.1 dB) yield diminishing returns. Lower margins increase user throughput and handover rate, with reactive mechanisms being more sensitive to the change of this parameter than predictive ones.

- **Impact of λ on network preference:** The network selection coefficient λ modulates the system's bias towards RF connectivity. Below a certain threshold speed, lower λ values improve all metrics. Beyond this speed, the lower lambda values continue to enhance average user throughput but degrade 10^{th} percentile performance and increase handover rate. This threshold speed occurs earlier for reactive mechanisms than predictive ones. λ should therefore be tuned based on whether reliability or user throughput is the primary objective.

- **Behaviour of η across predictive methods:** The prediction window size η exhibits distinct behaviour in the two predictive mechanisms. For predictive SINR, η is speed-dependent, with larger values of η preferred at low speeds and smaller values at high speeds. This trade-off affects both user throughput and handover rate. For predictive throughput, η is decoupled from speed and instead aligns with t_{wait}, the network's decision interval. Values close to t_{wait} yield optimal performance.

- **Implications for indoor networks:** In typical indoor environments, user speeds rarely exceed 5 m/s. Below this threshold, optimising for average user throughput provides the greatest benefit, with manageable losses in 10^{th} percentile performance. Moreover, λ optimisation below this threshold improves both metrics simultaneously, allowing aggressive tuning for user throughput without compromising reliability.

6.2 Future work

Building upon the findings and limitations identified in this thesis, several directions for future research are proposed:

- **More realistic receiver models:** Research into receiver design for NB-OWC systems is ongoing. Evaluating the proposed mechanisms using state-of-the-art receivers would allow for the inclusion of additional environmental factors such as device orientation and receiver field-of-view

(FOV), potentially revealing new performance constraints or opportunities.

- **Variable channel conditions:** The current optical network is modelled without channel variance, meaning that metrics such as SINR and user throughput remain consistent at a given location over time. As a result, handovers are triggered solely by user mobility. Incorporating stochastic effects, such as random beam blockages or orientation changes, would provide a more realistic evaluation of mechanism performance under dynamic conditions.

- **Alternative trajectory prediction mechanisms:** Presently, location prediction is based on linear trajectory estimation, which performs well at low speeds but is sensitive to abrupt direction changes at higher speeds. Exploring alternative prediction strategies, including machine learning-based models, could improve accuracy in forecasting non-linear user movement.

- **Realistic handover overhead time analysis:** The current framework assumes minimal overhead beyond dwell time (reactive) and wait time (predictive), effectively treating handovers as instantaneous. In practice, switching between beams or access points may incur additional delays. Incorporating realistic handover overhead times into the simulation could reveal whether handover rate becomes a bottleneck for overall performance.

- **Alternative hybrid network configurations:** This thesis employs Wi-Fi as the RF component due to its prevalence in HLWNet literature. However, in NB-OWC systems, the disparity in user throughput between optical and RF networks diminishes the role of the RF fallback. Investigating RF technologies with higher user throughput potential may yield new insights into parameter interactions and handover dynamics.

- **Extension to multi-user scenarios:** Expanding the simulation framework to support multiple users would enable the study of contention, interference, and fairness among users. This would also allow for the evaluation of scheduling and resource allocation strategies in hybrid NB-OWC/RF networks.

These directions aim to further improve the scalability, adaptability, and practicality of mobility-aware handover mechanisms in next-generation hybrid OWC/RF networks.

Bibliography

[1] Ansys Zemax OpticStudio | Optical Design and Analysis Software.

[2] Cisco Annual Internet Report - Cisco Annual Internet Report (2018–2023) White Paper.

[3] Public Wi-Fi Market Size | Mordor Intelligence.

[4] Recommendation ITU-R M.2160-0 (11/2023) - Framework and overall objectives of the future development of IMT for 2030 and beyond.

[5] Occupational exposure to ultraviolet radiation. 1972. Place: Cincinnati, OH].

[6] Short range optical interconnection. In Saša Radovanović, Anne-Johan Annema, and Bram Nauta, editors, *High-Speed Photodiodes in Standard CMOS Technology*, pages 7–31. Springer US, Boston, MA, 2006.

[7] Safety of laser products - Part 1: Equipment classification and requirements, May 2014.

[8] Jeremiah O. Abolade, Olasebikan A. Fakolujo, and Abidemi Orimogunje. Handover in Mobile Wireless Communication Network - A Review. *International Journal of Advanced Engineering, Management and Science*, 3(9):934–940, 2017. Publisher: AI Publications.

[9] Sakshi Aggarwal. Development and Assessment of Resource Management Solutions for Throughput Enhancement in a RIS-aided Mobile Network. Master's thesis, TU Delft, 2023.

[10] Imtiaz Ahamed Apon, Md. Ratul Hasan, Ibrahim Khalil, Md. Aminuzzman, Md. Samiul Islam, and Md. Ferdoush Wahid. FIR-FSOC in Challenging Atmospheric Conditions Considering Various Modulation Scheme. In *2024 International Conference on Control, Computing, Communication and Materials (ICCCCM)*, pages 442–447, August 2024.

[11] Xu Bao, Jisheng Dai, and Xiaorong Zhu. Visible light communications heterogeneous network (VLC-HetNet): new model and protocols for mobile scenario. *Wireless Networks*, 23(1):299–309, January 2017.

[12] D.L. Begley. "Free-space laser communications: a historical perspective". In *The 15th Annual Meeting of the IEEE Lasers and Electro-Optics Society*, volume 2, pages 391–392 vol.2, November 2002. ISSN: 1092-8081.

[13] Toni Besjedica, Krešimir Fertalj, Vlatko Lipovac, and Ivona Zakarija. Evolution of Hybrid LiFi–WiFi Networks: A Survey. *Sensors*, 23(9):4252, January 2023. Number: 9 Publisher: Multidisciplinary Digital Publishing Institute.

[14] Jenila C. and Jeyachitra R.K. Design of Green Indoor IoT Networking Through Optical Wireless Communication Using Passive Optical Reflectors. In *2018 IEEE Recent Advances in Intelligent Computational Systems (RAICS)*, pages 159–163, December 2018.

[15] Willy Anugrah Cahyadi, Yong Hyeon Kim, Yeon Ho Chung, and Chang-Jun Ahn. Mobile Phone Camera-Based Indoor Visible Light Communications With Rotation Compensation. *IEEE Photonics Journal*, 8(2):1–8, April 2016.

[16] V.W.S. Chan. Optical satellite networks. *Journal of Lightwave Technology*, 21(11):2811–2827, November 2003.

[17] Naresh Chand, Todd DeLuck, J. Hunton Andrew, Bruce M. Eteson, T. Moriarty Daniel, and Robert T. Carlson. Compact low-cost non-RF communication solutions for unmanned ground vehicles. In *2010 - MILCOM 2010 MILITARY COMMUNICATIONS CONFERENCE*, pages 1577–1582, October 2010. ISSN: 2155-7586.

[18] Aizaz U. Chaudhry and Halim Yanikomeroglu. Laser Intersatellite Links in a Starlink Constellation: A Classification and Analysis. *IEEE Vehicular Technology Magazine*, 16(2):48–56, June 2021.

[19] Ludovic Chevalier, Stephanie Sahuguede, and Anne Julien-Vergonjanne. Optical Wireless Links as an Alternative to Radio-Frequency for Medical Body Area Networks. *IEEE Journal on Selected Areas in Communications*, 33(9):2002–2010, September 2015.

[20] Mostafa Chowdhury, Moh Khalid Hasan, Md Shahjalal, Md Tanvir Hossan, and Yeong Min Jang. Optical Wireless Hybrid Networks: Trends, Opportunities, Challenges, and Research Directions. *IEEE Communications Surveys & Tutorials*, PP:1–1, January 2020.

[21] Mostafa Chowdhury, Md Tanvir Hossan, Amirul Islam, and Yeong Min Jang. A Comparative Survey of Optical Wireless Technologies: Architectures and Applications. *IEEE Access*, PP:1–1, January 2018.

[22] Kaiyun Cui, Gang Chen, Zhengyuan Xu, and Richard D. Roberts. Line-of-sight visible light communication system design and demonstration. In *2010 7th International Symposium on Communication Systems, Networks & Digital Signal Processing (CSNDSP 2010)*, pages 621–625, July 2010.

[23] Svilen Dimitrov, Raed Mesleh, Harald Haas, Mario Cappitelli, Michael Olbert, and Erhard Bassow. Path Loss Simulation of an Infrared Optical Wireless System for Aircrafts. In *GLOBECOM 2009 - 2009 IEEE Global Telecommunications Conference*, pages 1–6, November 2009. ISSN: 1930-529X.

[24] Hany Elgala, Raed Mesleh, and Harald Haas. Indoor optical wireless communication: potential and state-of-the-art. *IEEE Communications Magazine*, 49(9):56–62, September 2011.

[25] Lifang Feng, Rose Qingyang Hu, Jianping Wang, Peng Xu, and Yi Qian. Applying VLC in 5G Networks: Architectures and Key Technologies. *IEEE Network*, 30(6):77–83, November 2016.

[26] F.R. Gfeller and U. Bapst. Wireless in-house data communication via diffuse infrared radiation. *Proceedings of the IEEE*, 67(11):1474–1486, November 1979.

[27] Zabih Ghassemlooy, Pengfei Luo, and Stanislav Zvanovec. Optical Camera Communications. In Murat Uysal, Carlo Capsoni, Zabih Ghassemlooy, Anthony Boucouvalas, and Eszter Udvary, editors, *Optical Wireless Communications: An Emerging Technology*, pages 547–568. Springer International Publishing, Cham, 2016.

[28] A.J. Goldsmith and Soon-Ghee Chua. Variable-rate variable-power MQAM for fading channels. *IEEE Transactions on Communications*, 45(10):1218–1230, October 1997.

[29] Liang Guo, Yanan Guo, Junxi Wang, and Tongbo Wei. Ultraviolet communication technique and its application. *Journal of Semiconductors*, 42(8):081801, August 2021. Publisher: Chinese Institute of Electronics.

[30] Harald Haas and Cheng Chen. What is LiFi? In *2015 European Conference on Optical Communication (ECOC)*, pages 1–3, September 2015.

[31] Harold Haas. High-speed wireless networking using visible light | SPIE, the international society for optics and photonics: SPIE, 2013.

[32] Eugene Hecht. *Optics*. Addison-Wesley, 2002. Google-Books-ID: T3ofAQAAMAAJ.

[33] J. Hou and D.C. O'Brien. Vertical handover-decision-making algorithm using fuzzy logic for the integrated Radio-and-OW system. *IEEE Transactions on Wireless Communications*, 5(1):176–185, 2006.

[34] Pengfei Hu, Parth H. Pathak, Aveek K. Das, Zhicheng Yang, and Prasant Mohapatra. PLiFi: hybrid wifi-VLC networking using power lines. In *Proceedings of the 3rd Workshop on Visible Light Communication Systems*, VLCS '16, pages 31–36, New York, NY, USA, October 2016. Association for Computing Machinery.

[35] Gazi Zahirul Islam. Throughput Analysis of Wireless Local Area Network. 6(4), 2016.

[36] Shinya Itoh, Isamu Takai, Md. Shakowat Zaman Sarker, Moeta Hamai, Keita Yasutomi, Michinori Andoh, and Shoji Kawahito. A CMOS image sensor for 10Mb/s 70m-range LED-based spatial optical communication. In *2010 IEEE International Solid-State Circuits Conference - (ISSCC)*, pages 402–403, February 2010. ISSN: 2376-8606.

[37] Han Ji, Qiang Wang, Stephen J. Redmond, Iman Tavakkolnia, and Xiping Wu. Adaptive Target-Condition Neural Network: DNN-Aided Load Balancing for Hybrid LiFi and WiFi Networks, August 2022. arXiv:2208.05035 [eess].

[38] David B. Johnson and David A. Maltz. Dynamic Source Routing in Ad Hoc Wireless Networks. In Tomasz Imielinski and Henry F. Korth, editors, *Mobile Computing*, volume 353, pages 153–181. Springer US, Boston, MA, 1996. Series Title: The Kluwer International Series in Engineering and Computer Science.

[39] Juan C. Juarez, Anurag Dwivedi, A. Roger Hammons, Steven D. Jones, Vijitha Weerackody, and Robert A. Nichols. Free-Space Optical Communications for Next-generation Military Networks. *IEEE Communications Magazine*, 44(11):46–51, November 2006.

[40] J.M. Kahn, W.J. Krause, and J.B. Carruthers. Experimental characterization of non-directed indoor infrared channels. *IEEE Transactions on Communications*, 43(2/3/4):1613–1623, February 1995. Conference Name: IEEE Transactions on Communications.

[41] Hossein Kazemi, Elham Sarbazi, Michael Crisp, Taisir E. H. El-Gorashi, Jaafar M. H. Elmirghani, Richard V. Penty, Ian H. White, Majid Safari, and Harald Haas. A Novel Terabit Grid-of-Beam Optical Wireless Multi-User Access Network With Beam Clustering, April 2024. arXiv:2404.04443 [eess].

[42] Hossein Kazemi, Elham Sarbazi, Michael Crisp, Taisir E. H. El-Gorashi, Jaafar M. H. Elmirghani, Richard V. Penty, Ian H. White, Majid Safari, and Harald Haas. A Novel Terabit Grid-of-Beam Optical Wireless Multi-User Access Network With Beam Clustering, April 2024. arXiv:2404.04443 [eess].

[43] Hossein Kazemi, Elham Sarbazi, Majid Safari, and Harald Haas. Multi-Beam Access Point Design for 6G Laser-Based Optical Wireless Networks: Eye Safety-Coverage Tradeoff. In *GLOBECOM 2023 - 2023 IEEE Global Communications Conference*, pages 5543–5548, December 2023. ISSN: 2576-6813.

[44] Mohammad Ali Khalighi and Murat Uysal. Survey on Free Space Optical Communication: A Communication Theory Perspective. *IEEE Communications Surveys & Tutorials*, 16(4):2231–2258, 2014.

[45] Dennis Killinger. Free Space Optics for Laser Communication Through the Air. *Optics and Photonics News*, 13(10):36–42, October 2002. Publisher: Optica Publishing Group.

[46] T. Komine and M. Nakagawa. Fundamental analysis for visible-light communication system using LED lights. *IEEE Transactions on Consumer Electronics*, 50(1):100–107, February 2004.

[47] Ton Koonen, Fausto Gomez-Agis, Zizheng Cao, Ketemaw Mekonnen, Frans Huijskens, and Eduward Tangdiongga. Indoor ultra-high capacity optical

wireless communication using steerable infrared beams. In *2017 International Topical Meeting on Microwave Photonics (MWP)*, pages 1–4, October 2017.

[48] Ton Koonen and Ketema Mekonnen. Recent Progress in High-capacity Optical Wireless Communication. In *2022 Asia Communications and Photonics Conference (ACP)*, pages 1819–1822, November 2022.

[49] Ton Koonen, Ketemaw Mekonnen, Zizheng Cao, Frans Huijskens, Ngoc Quan Pham, and Eduward Tangdiongga. Ultra-high-capacity wireless communication by means of steered narrow optical beams. *Philosophical transactions. Series A, Mathematical, physical, and engineering sciences*, 378(2169):20190192, April 2020.

[50] Ton Koonen, Joanne Oh, Ketemaw Mekonnen, Zizheng Cao, and Eduward Tangdiongga. Ultra-High Capacity Indoor Optical Wireless Communication Using 2D-Steered Pencil Beams. *Journal of Lightwave Technology*, 34(20):4802–4809, October 2016.

[51] Aravindh Krishnamoorthy, Hossein Safi, Othman Younus, Hossein Kazemi, Isaac N. O. Osahon, Mingqing Liu, Yi Liu, Sina Babadi, Rizwana Ahmad, Asim Ihsan, Behnaz Majlesein, Yifan Huang, Johannes Herrnsdorf, Sujan Rajbhandari, Jonathan J. D. McKendry, Iman Tavakkolnia, Humeyra Caglayan, Henning Helmers, Graham Turnbull, Ifor D. W. Samuel, Martin D. Dawson, Robert Schober, and Harald Haas. Optical Wireless Communications: Enabling the Next-Generation Network of Networks. *IEEE Vehicular Technology Magazine*, 20(2):20–39, June 2025.

[52] Yun Li, Bin Cao, and Chonggang Wang. Handover schemes in heterogeneous LTE networks: challenges and opportunities. *IEEE Wireless Communications*, 23(2):112–117, 2016.

[53] Research and Markets ltd. Wi-Fi 6 and Wi-Fi 6E Market Outlook for Key Devices (CPEs, Smartphones, Tablets, Laptops & PCs, Computer Accessories, AR/VR Headsets, Wireless Camera, Gaming Devices, Smart Home Devices, Automobile, Mobile Robots, Drones, Wearables, M2M Communication) - Global Forecast Till 2026.

[54] Hai-Han Lu, Chung-Yi Li, Hwan-Wei Chen, Chun-Ming Ho, Ming-Te Cheng, Zih-Yi Yang, and Chang-Kai Lu. A 56 Gb/s PAM4 VCSEL-Based LiFi Transmission With Two-Stage Injection-Locked Technique. *IEEE Photonics Journal*, 9(1):1–8, February 2017.

[55] Guanghui Ma, Mohammad Khalili, Rajendran Parthiban, and Marcos Katz. A Low-Complexity Handover Scheme Using Unsupervised Learning Techniques for 6G Multi-Networking. In *2023 2nd International Conference on 6G Networking (6GNet)*, pages 1–5, October 2023.

[56] Guanghui Ma, Rajendran Parthiban, and Nemai Karmakar. An Adaptive Handover Scheme for Hybrid LiFi and WiFi Networks. *IEEE Access*, 10:18955–18965, 2022. Conference Name: IEEE Access.

[57] Rainer Michalzik. VCSEL Fundamentals. *VCSELs, Springer Series in Optical Sciences, Volume 166. ISBN 978-3-642-24985-3. Springer-Verlag Berlin Heidelberg, 2013, p. 19*, 166:19, October 2013.

[58] Mahmood Naghshineah and Joseph M Kahn. Wireless Infrared Communication Systems and Networks. *International Journal of Wireless Information Networks*, 4(4):257–258, October 1997.

[59] Dominic C. O'Brien, Lubin Zeng, Hoa Le-Minh, Grahame Faulkner, Joachim W. Walewski, and Sebastian Randel. Visible light communications: Challenges and possibilities. In *2008 IEEE 19th International Symposium on Personal, Indoor and Mobile Radio Communications*, pages 1–5, September 2008. ISSN: 2166-9589.

[60] Ata Saygın Odabaşı, Onur İşçi, and Volkan Rodoplu. Machine Learning Based Seamless Vertical Handoff Mechanism for Hybrid Li-Fi/Wi-Fi Networks. In *2022 International Conference on INnovations in Intelligent SysTems and Applications (INISTA)*, pages 1–6, August 2022. ISSN: 2768-7295.

[61] Y. Oike, M. Ikeda, and K. Asada. A smart image sensor with high-speed feeble ID-beacon detection for augmented reality system. In *ESSCIRC 2004 - 29th European Solid-State Circuits Conference*, pages 125–128, September 2003.

[62] Eldad Perahia. Next generation wireless LANs : 802.11n, 802.11ac /, 2013. Place: Cambridge ; Publisher: Cambridge University Press,.

[63] Ngoc Quan Pham, Ketemaw Mekonnen, Eduward Tangdiongga, Ali Mefleh, and Ton Koonen. Efficient Mobility Management for Indoor Optical Wireless Communication System. *IEEE Photonics Technology Letters*, 33(17):939–942, September 2021.

[64] Michael B. Rahaim, Anna Maria Vegni, and Thomas D. C. Little. A hybrid Radio Frequency and broadcast Visible Light Communication system. In *2011 IEEE GLOBECOM Workshops (GC Wkshps)*, pages 792–796, December 2011. ISSN: 2166-0077.

[65] Bahaa Saleh and Teich Malvin. *Fundamentals of Photonics,*, volume 1. 3rd edition, February 2019.

[66] Elham Sarbazi, Hossein Kazemi, Michael Crisp, Taisir El-Gorashi, Jaafar Elmirghani, Richard V. Penty, Ian H. White, Majid Safari, and Harald Haas. Design and Optimization of High-Speed Receivers for 6G Optical Wireless Networks. *IEEE Transactions on Communications*, 72(2):971–990, February 2024.

[67] Elham Sarbazi, Hossein Kazemi, Mohammad Dehghani Soltani, Majid Safari, and Harald Haas. A Tb/s Indoor Optical Wireless Access System Using VCSEL Arrays. In *2020 IEEE 31st Annual International Symposium on Personal, Indoor and Mobile Radio Communications*, pages 1–6, August 2020. ISSN: 2166-9589.

[68] Tishya Sarma Sarkar, Bappaditya Sinha, Shibabrata Mukherjee, Indranuj Joardar, and Saswati Mazumdar. Development of an FPGA based Indoor Free Space Optical (FSO) Communication System using 808 nm Infrared (IR) LASER Source. In *2020 IEEE Calcutta Conference (CALCON)*, pages 313–317, February 2020.

[69] Antonios Seas, Bryan Robinson, Tina Shih, Farzana Khatri, and Mark Brumfield. Optical communications systems for NASA's human space flight missions. In Nikos Karafolas, Zoran Sodnik, and Bruno Cugny, editors, *International Conference on Space Optics — ICSO 2018*, page 16, Chania, Greece, July 2019. SPIE.

[70] Chen Sun, Xiqi Gao, Jiaheng Wang, Zhi Ding, and Xiang-Gen Xia. Beam Domain Massive MIMO for Optical Wireless Communications With Transmit Lens. *IEEE Transactions on Communications*, 67(3):2188–2202, March 2019.

[71] Wen-Shing Tsai, Hai-Han Lu, Chung-Yi Li, Ting-Chieh Lu, Chen-Hong Liao, Chien-An Chu, and Peng-Chun Peng. A 20-m/40-Gb/s 1550-nm DFB LD-Based FSO Link. *IEEE Photonics Journal*, 7(6):1–7, December 2015.

[72] Dobroslav Tsonev, Stefan Videv, and Harald Haas. Towards a 100 Gb/s visible light wireless access network. *Optics Express*, 23(2):1627–1637, January 2015. Publisher: Optica Publishing Group.

[73] Stefan Videv and Harald Haas. Hybrid Visible Light and Radio Frequency Communication Systems. *2014 IEEE 79th Vehicular Technology Conference (VTC Fall)*, 2014.

[74] Ke Wang, Zeshi Yuan, Elaine Wong, Kamal Alameh, Hongtao Li, Kandeepan Sithamparanathan, and Efstratios Skafidas. Experimental Demonstration of Indoor Infrared Optical Wireless Communications With a Silicon Photonic Integrated Circuit. *Journal of Lightwave Technology*, 37(2):619–626, January 2019.

[75] Xiping Wu, Cheng Chen, and Harald Haas. Mobility Management for Hybrid LiFi and WiFi Networks in the Presence of Light-Path Blockage. In *2018 IEEE 88th Vehicular Technology Conference (VTC-Fall)*, pages 1–5, August 2018. ISSN: 2577-2465.

[76] Xiping Wu and Dominic C. O'Brien. A Novel Machine Learning-Based Handover Scheme for Hybrid LiFi and WiFi Networks. In *2020 IEEE Globecom Workshops (GC Wkshps*, pages 1–5, December 2020.

[77] Xiping Wu and Dominic C. O'Brien. A Novel Machine Learning-Based Handover Scheme for Hybrid LiFi and WiFi Networks. In *2020 IEEE Globecom Workshops (GC Wkshps*, pages 1–5, December 2020.

[78] Xiping Wu, Dominic C. O'Brien, Xiong Deng, and Jean-Paul M. G. Linnartz. Smart Handover for Hybrid LiFi and WiFi Networks. *IEEE Transactions on Wireless Communications*, 19(12):8211–8219, December 2020. Conference Name: IEEE Transactions on Wireless Communications.

[79] Xiping Wu, Mohammad Dehghani Soltani, Lai Zhou, Majid Safari, and Harald Haas. Hybrid LiFi and WiFi Networks: A Survey, January 2020. arXiv:2001.04840 [cs].

[80] Xiping Wu, Mohammad Dehghani Soltani, Lai Zhou, Majid Safari, and Harald Haas. Hybrid LiFi and WiFi Networks: A Survey. *IEEE Communications Surveys & Tutorials*, 23(2):1398–1420, 2021.

[81] Zhengyuan Xu and Brian M. Sadler. Ultraviolet Communications: Potential and State-Of-The-Art. *IEEE Communications Magazine*, 46(5):67–73, May 2008.

[82] Takaya Yamazato, Isamu Takai, Hiraku Okada, Toshiaki Fujii, Tomohiro Yendo, Shintaro Arai, Michinori Andoh, Tomohisa Harada, Keita Yasutomi, Keiichiro Kagawa, and Shoji Kawahito. Image-sensor-based visible light communication for automotive applications. *IEEE Communications Magazine*, 52(7):88–97, July 2014.

[83] Yi Liu, Ali Wajahat, Rui Chen, Nikos Bamiedakis, Michael Crisp, Ian H. White, and Richard V. Penty. High-capacity optical wireless VCSEL array transmitter with uniform coverage. volume 12413, page 124130J, March 2023.

[84] Zhihong Zeng, Mohammad Dehghani Soltani, Majid Safari, and Harald Haas. A VCSEL Array Transmission System With Novel Beam Activation Mechanisms. *IEEE Transactions on Communications*, 70(3):1886–1900, March 2022. Conference Name: IEEE Transactions on Communications.

[85] Zhengyuan Xu, Gang Chen, Feras Abou-Galala, and Michael Leonardi. Experimental performance evaluation of non-line-of-sight ultraviolet communication systems. volume 6709, page 67090Y, September 2007.

Appendix A

Modifications to NB-OWC reference model

This appendix investigates the deviations observed between the simulated intensity distribution and the reference model presented in [41]. While the simulation framework adheres to the mathematical formulation provided in the paper, the resulting coverage pattern exhibits notable asymmetries and beam convergence effects not present in the original distribution. Through comparative analysis, step-by-step validation, and targeted parameter modifications, this chapter identifies the source of these discrepancies and outlines the adjustments made to align the simulation output more closely with the intended design.

A.1 Comparison of intensity distributions

The modelling of the NB-OWC system is provided by the detailed mathematical framework described in [41]. However, when implemented using the default parameters outlined in Table 1 of the paper, the resulting normalized intensity distribution deviates noticeably from the reference image presented in the paper (see Figure A.1).

Several discrepancies are can be observed:

- **Coverage Area:** The reference distribution spans the entire 5×5 m coverage area, whereas the implementation fails to do so. This suggests that the beam divergence does not match the intended design, even though the placement of the VCSELs and lenses is accurate.
- **Beam Convergence:** In the simulated distribution, certain regions exhibit high beam convergence, where multiple beams overlap significantly. This is in contrast to the reference distribution, where beams remain distinct. A notable example is around the coordinate $(0.75, 0.75)$, where the implementation shows a single circular beam, while the reference clearly distinguishes four separate beams.
- **Relative Intensity Scaling:** Due to the convergence mentioned above, the total intensity at overlapping zones in the implementation is disproportionately high. Since the distribution is normalized, these peaks compress

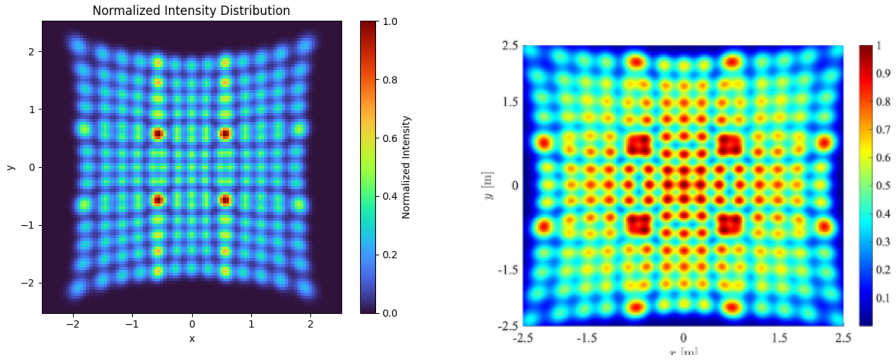

(a) **Normalized intensity distribution generated by simulator**

(b) **Normalized intensity distribution given by Kazemi et al. [41]**

Figure A.1: **Comparison of normalized intensity distribution between implementation and reference.**

the relative scale of the remaining regions. As a result, non-overlapping areas appear with reduced relative contrast compared to the reference distribution. In contrast, the greater beam divergence in the reference leads to lower peak values and a more uniform distribution of intensity across the coverage area.

The most significant discrepancy arises from the symmetry of the distribution (see Figure A.2). In the implementation, the distribution is symmetric across both the horizontal and vertical axes, meaning that the intensity pattern is mirrored when flipped left–right or top–bottom. However, the distribution is not symmetric across the diagonal. This becomes apparent when comparing the coverage along the two axes: the horizontal axis spans from -2 to 2 m, while the vertical axis spans from -2.25 to 2.25 m.

This asymmetry is unexpected, given that the VCSEL and lens arrangement is symmetrical across all axes. Therefore, the resulting beam distribution should also exhibit full symmetry. The observed deviation suggests a flaw in the beam generation process, which will be investigated in the following section.

A.2 Beam generation process

The process of calculating the projection vector of the beam generated by a VCSEL can be divided into two distinct stages: the computation of the *relative projection* and the *absolute projection*.

Relative projection

The relative projection refers to the unit direction vector of the beam immediately after it is refracted by the plano-convex lens, assuming the VCSEL is oriented straight downward (i.e., aligned with the optical axis). This is illustrated in Figure A.3.

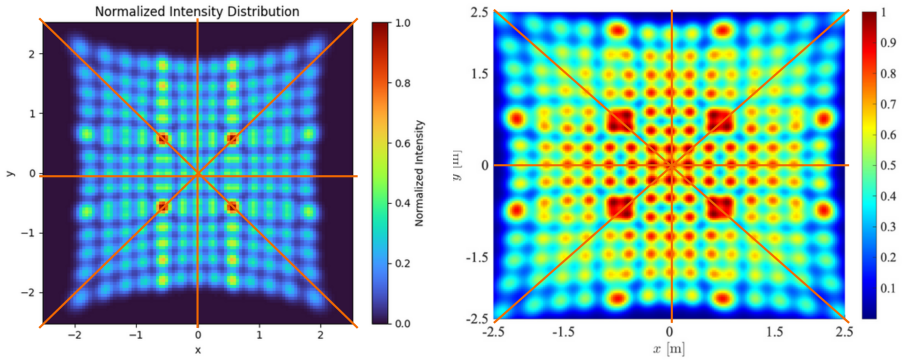

Figure A.2: **Symmetry comparison between implementation and reference.**

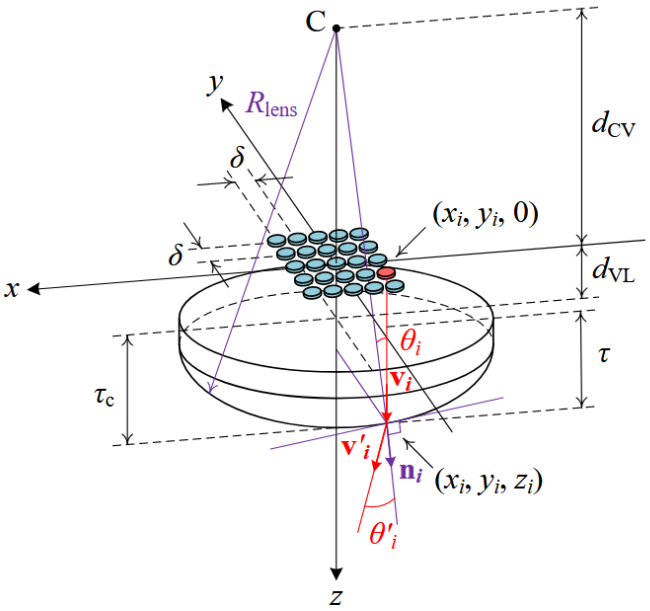

Figure A.3: **3D modelling of a transmitter element. Light refraction through the plano-convex lens for the ith VCSEL [42]**

The coordinates of the ith VCSEL in its local array are computed using Equations (10a) and (10b) from [41]

$$x_i = (-3 + n)\delta, \tag{A.1}$$
$$y_i = (3 - m)\delta, \tag{A.2}$$

where $m = \left\lceil \frac{i}{5} \right\rceil$ and $n = i - 5(m - 1)$, and δ is the pitch distance between VCSELs.

Using these coordinates, the relative projection vector $\mathbf{v}'_i$ is calculated based on the law of refraction and lens geometry, as given in Equations (16) and (17) as

$$\mathbf{v}'_i = Qx_i\mathbf{n}_x + Qy_i\mathbf{n}_y + \left(n_{\text{lens}} + Q\sqrt{R^2_{\text{lens}} - x_i^2 - y_i^2}\right)\mathbf{n}_z, \tag{A.3}$$

where Q is defined as

$$Q = \frac{\sqrt{R^2_{\text{lens}} - n^2_{\text{lens}}(x_i^2 + y_i^2)} - n_{\text{lens}}\sqrt{R^2_{\text{lens}} - x_i^2 - y_i^2}}{R^2_{\text{lens}}}. \tag{A.4}$$

Here, R_{lens} is the radius of curvature of the plano-convex lens, and n_{lens} is its refractive index.

Absolute projection

The absolute projection accounts for the orientation of the transmitter element to which the VCSEL belongs. Each transmitter element in the double-tier AP is tilted by a specific angle to ensure full coverage of the receiver plane.

To obtain the final unit projection vector in the global coordinate system, the relative projection vector $\mathbf{v}'_i$ is transformed using a series of Euler rotation matrices, described in Equation (28) as

$$\mathbf{v}'_j = R_y(\beta_v)R_x(\alpha_v)\mathbf{v}'_i, \tag{A.5}$$

where α_v and β_v are the tilt angles of the vth transmitter element about the x and y axes, respectively.

The rotation matrices are defined as

$$R_x(\alpha_v) = \begin{bmatrix} 1 & 0 & 0 \\ 0 & \cos\alpha_v & -\sin\alpha_v \\ 0 & \sin\alpha_v & \cos\alpha_v \end{bmatrix}, \tag{A.6}$$

$$R_y(\beta_v) = \begin{bmatrix} \cos\beta_v & 0 & \sin\beta_v \\ 0 & 1 & 0 \\ -\sin\beta_v & 0 & \cos\beta_v \end{bmatrix}. \tag{A.7}$$

This two-step process supposedly ensures that each beam is accurately projected into the simulation space, accounting for both the optical transformation through the lens and the physical orientation of the transmitter element.

Validation and investigation of asymmetry

To identify the source of asymmetry in the beam projection pattern, a series of tests were conducted to isolate each transformation step in the beam generation pipeline.

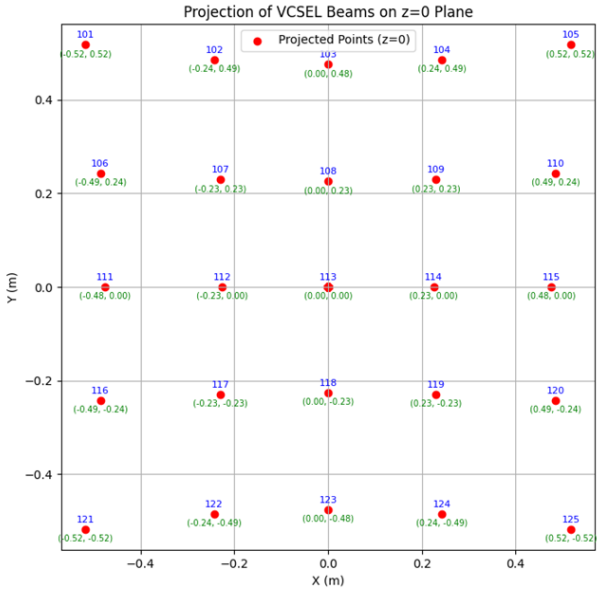

Figure A.4: **Projection of beams on the receiver plane from the 25 VCSELs of transmitter element 5. The numbers indicate the VCSEL index.**

Test 1: Central transmitter element (Element 5) The first test examined the projection pattern of the 25 VCSELs belonging to transmitter element 5. This element is oriented directly downward, with zero tilt angles about both the x and y axes. Consequently, the rotation matrices reduce to identity matrices, and the absolute projection is identical to the relative projection.

As shown in Figure A.4, the projection pattern generated by this element exhibit symmetry across all axes. This confirms that the mechanism used to generate the relative projection vectors is accurate. Moreover, since the relative projection vectors are identical across all transmitter elements prior to rotation, the observed asymmetry must originate in the transformation to absolute projection.

Test 2: Corner transmitter element (Element 1) The second test considered transmitter element 1, located at a corner of the array. This element has non-zero tilt angles about both the x and y axes. As shown in Figure A.5, the resulting projection pattern lacks diagonal symmetry. Since the relative projection vectors are symmetrical, this indicates that the transformation step using Euler rotation matrices is the source of the asymmetry.

Test 3: VCSEL index 225 To further validate this observation, the relative and absolute projection vectors were examined for VCSEL index 225, corresponding to the bottom-left VCSEL in the array. The relative projection retains

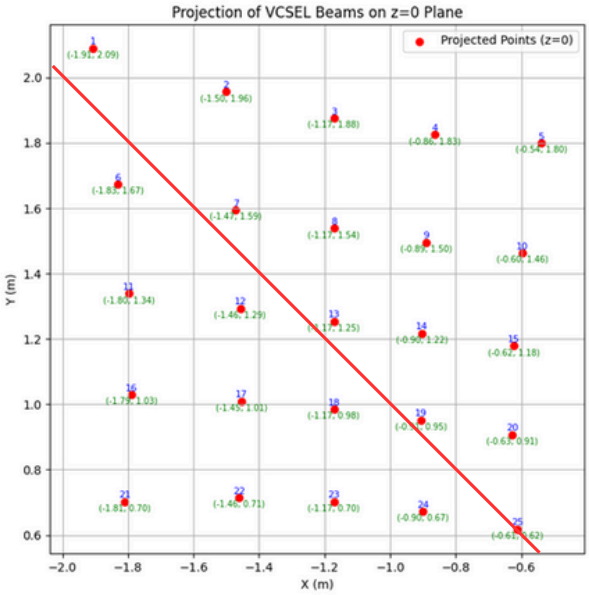

Figure A.5: **Projection of beams on the receiver plane from the 25 VCSELs of transmitter element 1 with diagonal axis of symmetry.**

symmetry with respect to both the x- and y-axes, consistent with the expected geometry. In contrast, the absolute projection breaks this symmetry, confirming that the asymmetry originates in the transformation process rather than in the generation of the relative vectors.

These tests collectively demonstrate that the asymmetry observed in the simulated intensity distribution originates from the transformation step that computes the absolute projection vectors using Euler rotations.

A.3 Modification for improved distribution

Although achieving perfect symmetry in the intensity distribution is not feasible due to limitations in the analytical transformation model, it is still possible to compensate through parameter tuning to approximate the reference distribution more closely. This limitation stems from the analytical model rather than the physical system: simulations in Zemax[1] produce distributions consistent with the reference model [41], confirming that the asymmetry arises from the model equations rather than the system physics.

One of the most impactful modifications involves adjusting the tilt angles of the transmitter elements. In the original implementation, a tilt angle of 21° was used as suggested by the reference model. However, this configuration resulted in excessive beam convergence, where multiple VCSELs projected onto the same region of the receiver plane, creating high-intensity hotspots and reducing spatial coverage.

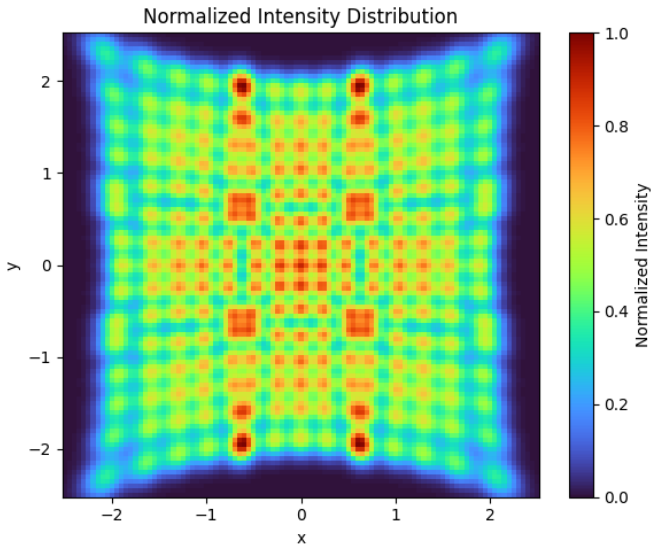

Figure A.6: **Normalised intensity distribution with parameter modification**

Increasing the tilt angle to 23° enhances beam divergence, effectively separating previously overlapping beams. As shown in Figure A.6, the modified configuration produces a distribution where the beams are more distinct, particularly in regions where four beams previously converged onto a single point.

This increased divergence reduces peak intensity at convergence zones and improves the overall spread of intensity across the receiver plane. As a result, the distribution is more balanced, with higher relative intensity in peripheral regions, closely resembling the reference distribution in [41].

Although the handover mechanism depends on the absolute intensity at specific user locations, the obtained normalised intensity distribution provides a realistic representation of a NB-OWC VCSEL array. Each VCSEL beam maintains its Gaussian intensity profile even after lens transformation, so local beam behaviour remains consistent. Therefore, despite the asymmetry in the overall distribution, it is justified to use this model to assess handover performance, as the algorithm is driven by individual beam intensities rather than the precise symmetry of the aggregate pattern.